NAVAL POSTGRADUATE SCHOOL

MONTEREY, CALIFORNIA

THESIS

APPLICATION OF COPPER INDIUM GALLIUM DISELENIDE PHOTOVOLTAIC CELLS TO EXTEND THE ENDURANCE AND CAPABILITIES OF THE RAVEN RQ-11B UNMANNED AERIAL VEHICLE

by

Javier V. Coba

September 2010

Thesis Advisor:	Sherif Michael
Second Reader:	Todd Weatherford

THIS PAGE INTENTIONALLY LEFT BLANK

REPORT DOCUMENTATION PAGE		Form Approved OMB No. 0704-0188

1. AGENCY USE ONLY *(Leave blank)*	2. REPORT DATE	3. REPORT TYPE AND DATES COVERED
	September 2010	Master's Thesis

4. TITLE AND SUBTITLE
Application of Copper Indium Gallium Diselenide Photovoltaic Cells to Extend the Endurance and Capabilities of the Raven RQ-11B Unmanned Aerial Vehicle

5. FUNDING NUMBERS

6. AUTHOR(S) Javier V. Coba

7. PERFORMING ORGANIZATION NAME(S) AND ADDRESS(ES)
Naval Postgraduate School
Monterey, CA 93943-5000

8. PERFORMING ORGANIZATION REPORT NUMBER

9. SPONSORING /MONITORING AGENCY NAME(S) AND ADDRESS(ES)
Unmanned Aerial Systems Weaponization Laboratory, Naval Air Warfare Center Weapons Division (NAWCWD) China Lake, CA

10. SPONSORING/MONITORING AGENCY REPORT NUMBER

11. SUPPLEMENTARY NOTES The views expressed in this thesis are those of the author and do not reflect the official policy or position of the Department of Defense or the U.S. Government. IRB Protocol number _____N/A_____.

12a. DISTRIBUTION / AVAILABILITY STATEMENT
Approved for public release; distribution is unlimited

12b. DISTRIBUTION CODE

13. ABSTRACT (maximum 200 words)

Prior thesis work has demonstrated the possibility of extending the flight time of military Small Unmanned Aerial Vehicles (SUAV) by 200% with the implementation of thin-film photovoltaic (TFPV) cells. In this thesis, we investigate how thin-film photovoltaic cells, made out of Copper Indium Gallium Di-Selenide (CIGS) semiconductor materials and mounted on the wings of the Raven RQ-11B SUAV, provide sufficient electrical power to fully operate the UAV for extended periods of time. This research focuses on extending the flight time of the Raven RQ-11B and on minimizing its sole dependence on lithium-ion batteries. This research will also demonstrate that increasing the size of the wings, adding a DC to DC power converter, and using a Maximum Power Point Tracker (MPPT) will enable the Raven RQ-11B to keep its lithium-ion battery charging continuously, while operating under varying daylight conditions. Additionally, this research will investigate the advantage of enabling systems on the ground to "self-charge." This will enable tactical units to operate in any field, to include areas where power sources are unavailable.

14. SUBJECT TERMS	15. NUMBER OF PAGES
Thin-Film Photovoltaics, CIGS, Unmanned Aerial Systems, UAV, Solar Panel, Maximum Power Point Tracker (MPPT), Lithium-ion	153
	16. PRICE CODE

17. SECURITY CLASSIFICATION OF REPORT	18. SECURITY CLASSIFICATION OF THIS PAGE	19. SECURITY CLASSIFICATION OF ABSTRACT	20. LIMITATION OF ABSTRACT
Unclassified	Unclassified	Unclassified	UU

NSN 7540-01-280-5500 Standard Form 298 (Rev. 2-89)
Prescribed by ANSI Std. 239-18

THIS PAGE INTENTIONALLY LEFT BLANK

Approved for public release; distribution is unlimited

APPLICATION OF COPPER INDIUM GALLIUM DISELENIDE PHOTOVOLTAIC CELLS TO EXTEND THE ENDURANCE AND CAPABILITIES OF THE RAVEN RQ-11B UNMANNED AERIAL VEHICLE

Javier V. Coba
Captain, United States Marine Corps
B.A., San Diego State University, 2004

Submitted in partial fulfillment of the
requirements for the degree of

MASTER OF SCIENCE IN ELECTRICAL ENGINEERING

from the

NAVAL POSTGRADUATE SCHOOL
September 2010

Author: Javier V. Coba

Approved by: Sherif Michael
Thesis Advisor

Todd Weatherford
Second Reader

Clark Robertson
Chairman, Department of Electrical and
Computer Engineering

THIS PAGE INTENTIONALLY LEFT BLANK

ABSTRACT

Prior thesis work has demonstrated the possibility of extending the flight time of military Small Unmanned Aerial Vehicles (SUAV) by 200% with the implementation of thin-film photovoltaic (TFPV) cells. In this thesis, we investigate how thin-film photovoltaic cells, made out of Copper Indium Gallium Di-Selenide (CIGS) semiconductor materials and mounted on the wings of the Raven RQ-11B SUAV, provide sufficient electrical power to fully operate the UAV for extended periods of time. This research focuses on extending the flight time of the Raven RQ-11B and on minimizing its sole dependence on lithium-ion batteries. This research will also demonstrate that increasing the size of the wings, adding a DC to DC power converter, and using a Maximum Power Point Tracker (MPPT) will enable the Raven RQ-11B to keep its lithium-ion battery charging continuously, while operating under varying daylight conditions. Additionally, this research will investigate the advantage of enabling systems on the ground to “self-charge.” This will enable tactical units to operate in any field, to include areas where power sources are unavailable.

THIS PAGE INTENTIONALLY LEFT BLANK

TABLE OF CONTENTS

THIS PAGE INTENTIONALLY LEFT BLANK

LIST OF FIGURES

LIST OF TABLES

EXECUTIVE SUMMARY

Since 2006, the Raven RQ-11B Unmanned Aerial Vehicle (UAV) has become the preferred miniature unmanned aerial vehicle (MUAV) used by the U.S. Army, USSOCOM, U.S. Marines, U.S. Air Force, and U.S. allies. The Raven unmanned aerial vehicle (UAV) characterizes itself by providing units with real-time color or infrared imagery, lightweight portability, long-range transmission, manual and programmable operation, etc., which make this type of aircraft a tremendous asset to units conducting low-altitude reconnaissance and surveillance missions.

Due to their higher energy density compared to other rechargeable batteries, the Raven RQ-11B uses one rechargeable lithium-ion battery for its full operation. Unfortunately, a fully charged lithium battery takes from 30 minutes to 1 hour to discharge. Therefore, the Raven UAV has a flight-time limitation that relates directly to the amount of time it takes for the battery to discharge. The battery is the only source of electrical power provided to the aircraft, and once the battery discharges, it forces the Raven operator to bring the aircraft back from its mission.

Another limitation encountered in the Raven UAV is its weight. Being a small unmanned aerial vehicle (SUAV), the aircraft is designed to lift a maximum weight of 4.2lb. Hence, there is no room to mount additional batteries to overcome the limited operating time that one battery provides. Besides, adding more batteries defeats the advantages of the SUAV, which is its portability. Soldiers and

Marines cannot add more weight to their already heavy packs to operate the Raven for more than 1 hour.

The objective of this research was to investigate an alternative way to provide constant electrical power to the Raven UAV and/or to recharge the embedded lithium-ion battery on the aircraft without adding additional batteries, and therefore, extending its endurance. For this, we looked at thin-film photovoltaic (TFPV) cells made out of copper indium gallium di-selenide (CIGS) semiconductor materials, with a power efficiency of 13%, to generate additional electric power from sunlight.

In the past, similar thesis work, performed on remotely piloted vehicles (RPV), has demonstrated that the flight time can be extended by three times with the use of TFPV. This thesis was designed to proof this concept on the Raven RQ-11B UAV, which is a heavier aircraft and whose power consumption is higher due to its payload.

Another part of the research consisted of using the wing-mounted solar cells to recharge UAV batteries or other electronics, reducing the need for an external power supply. One great advantage of using solar cells to recharge batteries or other electronics is the fact that it could do its job in absolute silence, preventing friendly forces from being detected by the enemy.

The improvement of endurance of the Raven could greatly benefit all military units who currently use this type of aircraft for intelligence, surveillance, and reconnaissance (ISR) missions. Additionally, this added capability could be of great interest in areas that require constant surveillance such as border, maritime, forestry, agriculture, etc.

LIST OF ACRONYMS AND ABBREVIATIONS

ACC/TYCOM	Aircraft Control Custodian Type Command
ACTD	Advanced Concept Technology Demonstration
AGL	Above Ground Level
Al	Aluminum
ALR	Automatic Launch and Recovery
a-Si	Amorphous Silicon
BCT	Brigade Combat Teams
BOIP	Basis Of Issue Plan
CBD	Chemical bath Deposition
CBE	Concept-Based Experimentation
CdS	Cadmium Sulfide
CdTe	Cadmium Telluride
CIGS	Cupper Indium Gallium Selenide
COTS	Commercial Off-The-Shelf
Cu	Cupper
DDL	Digital Data Link
DoD	Department of Defense
EO	Electro-Optical
FMV	Full Motion Video
FY	Fiscal Year
GCS	Ground Control Station
GCU	Ground Control Unit
GPS	Global Positioning System

IED	Improvised Explosive Devices
IR	Infra-red
ISR	Intelligence, Surveillance, Reconnaissance
Li-ion	Lithium Ion
Li-po	Lithium Polymer
LRIP	Low Rate Initial Production
MCE	Maneuver Center of Excellence
MCTSSA	Marine Corps Tactical Support Systems Activity
Mo	Molybdenum
MOUT	Military Operations in Urban Terrain
MPPT	Maximum Power Point Tracker
MTT	Mobile Training Teams
MUAV	Miniature Unmanned Aerial Vehicle
NETT	New Equipment Training Teams
Ni-Cd	Nickel Cadmium
NREL	National Renewable Energy Laboratory
OEF	Operation Enduring Freedom
OIF	Operation Iraqi Freedom
ORD	Operational Requirements Document
OSRVT	One System Remote Video Terminal
PM-UAS	Program Manager Unmanned Aerial Systems
POI	Program of Instruction
PVD	Physical Vapor Deposition
RPV	Remotely Piloted Vehicles
SOCOM	Special Operations Command

SC	Solar Cell
SP	Solar Panel
SUAV	Small Unmanned Aerial Vehicle
TFPV	Thin-Film Photovoltaic
TFSC	Thin-Film Solar Cells
TSP	Training Support Package
UAV	Unmanned Aerial Vehicle
UGV	Unmanned Ground Vehicles
UGS	Unattended Ground Sensors
USAACE	United States Army Aviation Center of Excellence
USMC	United States Marine Corps
USSOCOM	U.S. Special Operations Command
Wh	Watt hour
ZnO	Zinc Oxide

THIS PAGE INTENTIONALLY LEFT BLANK

ACKNOWLEDGMENTS

First, I would like to express my utmost gratitude to the most important persons in my life, my wife Doris, and children Andrew and Amy. Thank you for your unwavering support throughout the long hours and difficult times. Once again, you have made this journey an enjoyable experience.

Second, I would like to thank my thesis advisor, Dr. Sherif Michael, for his patience and assistance with this work. His knowledge on this subject was crucial to the successful accomplishment of this thesis work.

I would also like to thank Mr. Jeff Knight, John Mobley, and James Calusdian. Their technical support and expertise was instrumental to complete my design.

Lastly, I would like to thank Mr. Samuel Thompson, Andrew Tree, Scott Brown, Elijah Soto, Daniel Allen, and Mr. Felipe Jauregui, members of the Science & Technology Advanced Systems Unmanned Systems Activity at the Naval Air Warfare Center Weapons Division in China Lake, California, for providing me with a Raven RQ-11B asset to conduct my thesis, and for funding the entire project.

THIS PAGE INTENTIONALLY LEFT BLANK

I. INTRODUCTION

A. BACKGROUND

Small Unmanned Aerial Vehicles (SUAVs), small enough to be launched by hand and carried in a backpack, have proven to be a valuable asset for troops on the ground, specifically the Raven RQ-11B. Its portability and capability to expose enemy activity beyond the horizon, which otherwise would not be detected, make this Small Unmanned Aerial Vehicle (SUAV) a unique and essential piece of equipment for the military.

Several are the reasons that make the Raven UAV the preferred UAV of battalion commanders in Iraq and in Afghanistan. First, its operation is so simple that it does not require a highly trained pilot to fly it. Second, this aircraft is ideal for quick peeks to see what is on the other side of the obstructed terrain. Many Ravens are used to identify the location of Improvised Explosive Devices (IEDs). Third, their infra-red (IR) and Electro-Optical (EO) cameras provide enough resolution to show someone carrying a weapon. Some say that they are better than the cameras carried by the AH-64 Apache Attack Helicopter. Fourth, its price per unit is affordable compared to other large UAVs. Finally, its size and weight are perhaps the most attractive advantages, since it can be easily carried by Special Forces scouts and squads.

However, despite their enormous contributions in the battlefield, the Raven UAV, also known as a SUAV, has certain constraints that limit its operation. One of them is the partial amount of time the battery lasts on a single

mission. Each battery can provide a maximum of 90 minutes of flight, after which time the aircraft needs to be retrieved to recharge the battery. Unfortunately, for certain missions, one 1.5 hours is not enough time to conduct intelligence, surveillance, and reconnaissance (ISR) type operations, and adding more batteries represent more weight to the already heavy packs those soldiers and Marines carry on the battlefield. Therefore, it is imperative to look for alternative sources of energy to provide the Raven Small Unmanned Aerial Vehicle with additional power to conduct ISR operations for long periods of time without relying solely on batteries.

B. OBJECTIVE

Thanks to the recent advances in solar cell technology and the development of thin-film photovoltaic (TFPV) cells made out of CIGS semiconductor materials, the potential for replacing battery power with solar power on SUAV is greater every day. These lightweight, high efficiency, and flexible solar cells, mounted to the wings of the aircraft, could provide sufficient electrical power to operate the UAV without relying solely on battery power, thus, increasing the endurance and/or capabilities of the aircraft. In this research, we investigated the advantages of using sunlight as an alternative source of power for the Raven UAV.

Another part of this research included a small modification in the structure of the aircraft. By increasing the size of the center wing, we attempted to increase the lift, which reduces the amount of power provided by the battery, and at the same time, increases the area necessary to mount more solar cells.

Additionally, we tested Raven RQ-11B SUAV prior and during flight to determine the power consumption rate of the onboard lithium-ion battery at different speeds in order to identify different means to conserve electrical power and ways to recharge the battery while on flight. We also investigated the fact that, when the Raven is not in flight, wing-mounted solar cells can still be used to recharge other electronic equipment, reducing the need for troops to plug in to a power source or carry additional batteries.

Finally, this investigation took into consideration the cost benefit (increased flight time versus initial and recurring costs) of modifying the aircraft, as well as any other maintenance, training, special handling, storage needs, and potential negative impact on flight parameters.

C. RELATED WORK

On 4 November 1974, the Sunrise I (Figure 1), designed by R.J. Boucher from Astro Flight Inc., impressed many researchers around the world when his solar-powered aircraft flew 20 minutes at an altitude of around 100m during its inaugural flight.

Figure 1. Sunrise I, 1974 (From [1]).

Since then, close to a hundred flights have been conducted using solar technologies. The last successful solar UAV flight was reported on 17 July 2010, when the QinetiQ's Zephyr solar UAV completed a flight record of seven continuous days, breaking previous records [2]. Figure 2 shows a team of engineers and technicians preparing the Zephyr solar UAV for launch.

Figure 2. QinetiQ's Zephyr Solar UAV (From [2]).

Nowadays, more interesting ideas are in progress. For example, engineers are designing hybrid UAVs (fuel and solar power combined) that can be placed in geostationary position, above jet stream and above severe weather, where they can serve as telecommunications relays, weather observers, or peacekeepers over the horizon perch [3].

Nevertheless, this area of research is not limited to UAVs. Recently, researchers in Switzerland demonstrated the possibility of launching a solar-powered plane after they successfully launched their Solar Impulse with a pilot onboard, completing a 24 hour test flight over the skies of Switzerland. The carbon fiber prototype flew over a day, allowing its 12,000 solar panels to soak up as much energy

as possible, charging the batteries enough to keep the plane aloft through the dark of night [4].

On September 2009, [5] attempted a related type of research. Using a small commercial off-the-shelf (COTS) plane with similar characteristics to the Raven UAV, and mounting 8% efficient CIGS TFPV cells on the wings and with no additional electronic hardware such as a Maximum Power Point Tracker (MPPT) or power converter, he demonstrated that his plane could fly 2.5 times longer with solar cells than without. Hurd's research concluded that although the Raven is much heavier and has greater power consumption due to its payload, similar improvements could be seen using higher efficiency CIGS cells, a much improved construction, and a maximum power point tracker circuit. He also concluded that the cost of such solar modification is about 3% of the initial cost of a single Raven [5].

Our research is designed to apply the same concept to an actual Raven UAV and to improve its endurance and capability by modifying the structure of the aircraft, installing a maximum power point tracking circuit, and mounting 13% efficiency CIGS cells. With all these added parts, we expect the Raven RQ-11B to maintain, if not surpass, William Hurd's design and concept.

These previous discoveries gave us the confidence to continue our research and seek similar endurance results on smaller aircraft such as the Raven RQ-11B SUAV.

D. APPROACH

To even consider the possibility of conducting this research, it was imperative to get our hands around an ac-

tual Raven RQ-11B SUAV. Thanks to the Marines from Marine Corps Tactical Support Systems Activity (MCTSSA) and to the technical representatives from the Naval Weapons Center in China Lake, California, we were able to borrow one asset in which we were able to apply our concept.

Another important focus of this research was to explore the latest high-efficiency TFPV cells on the market. Global Solar, a German company, turned out to be our best vendor of solar cells for this project after they developed a 13% efficiency CIGS TFPV cell.

Similarly, DC-DC power converters, as well as maximum power point trackers and other electronic components, were necessary to investigate in order to improve the power consumption of the battery that powers the Raven SUAV.

Lastly, it was necessary to study the possibility of extending the size of the wing in order to improve its lift capacity. It is worth mentioning that this research focused on any modifications that would have the greatest operational impact for a significant number of years.

E. ORGANIZATION

- Chapter II reviews the Raven UAV Program and focuses on its acquisition, characteristics, and limitations, as well as capabilities.
- Chapter III reviews the theory of operation of solar cells, and compares available thin-film photovoltaic technology such as CIGS and Silicon.

- Chapter IV reviews different power electronic devices that needed to be integrated into the circuit in order to acquire the best possible output power from the solar panel.
- Chapter V covers the design and physical assembly of the aircraft components, as well as, its circuitry. Additionally, it reviews the construction of the modified wing along with other materials that were used to put the solar panel together.
- Chapter VI provides testing methods and results, to include bench tests, stationary outdoor, and flight tests.
- Chapter VII gives conclusions, and makes recommendations for future research.

THIS PAGE INTENTIONALLY LEFT BLANK

II. RAVEN RQ-11B UAV

A. HISTORY OF THE RAVEN PROGRAM

The Raven program started in 1999, when the U.S. Army acquired four FQM-151 Pointer UAVs from AeroVironment during Military Operations in Urban Terrain (MOUT) ACTD (Advanced Concept Technology Demonstration) program (FY98-02). The program was established to identify technology solutions to support dismounted forces fighting in urban terrain. The Army was looking for a lightweight, small, simple user interface, low cost, reliable and robust system [6]. The FQM-151 Pointer UAV operated by U.S. Marines is seen in Figure 3.

Figure 3. FQM-151 Pointer (From [7]).

Although the Pointer system provided that technology solution for gathering intelligence, it had some shortfalls that included the lack of an IR camera for night operations and a global positioning system (GPS). Additionally, its large ground control station (GCS) made the system unat-

tractive to commanders on the ground, due to its lack of portability. AeroVironment was, therefore, asked to develop a smaller station, and, in turn, the company also developed a smaller air vehicle, called Raven. It flew in October 2001, as a proof-of-concept vehicle named the "Flashlight" UAV [8].

Figure 4. Flashlight SUAV (From [9]).

In 2002, the Flashlight, seen in Figure 4, was developed into the Raven under the Army's "Pathfinder" ACTD program. The air vehicle was renamed Raven after the Norse God Odin's use of ravens for reconnaissance and later to the Pathfinder Raven. On 21 January 2003, the Vice Chief of Staff of the Army and the Army G-3 approved the 101st Airborne Division for the rapid acquisition and equipping/fielding of the Raven SUAV. The first Low-Rate Initial Production (LRIP) version was the modified Block I Raven, first delivered in May 2003. However, while testing the Block I UAVs, a couple of discrepancies were

encountered, including a difficult launch procedure and insufficient flight stability [6]. The Raven Block I is shown in Figure 5.

Figure 5. Raven Block I UAV (From [9]).

Corrections to these shortcomings were made in the Block II version, which was delivered in September 2003. The Block II was evaluated in Afghanistan, and the U.S. Special Operations Command eventually ordered a batch of 179 Raven systems with three UAVs each. The Raven Block II is seen in Figure 6. In late 2004, the official designation RQ-11A was allocated to the Raven air vehicle. Besides the size there was essentially no difference between the Raven RQ-11A and the FQM-151 Pointer. They both could carry the same navigation system, control equipment, and payload [6].

Figure 6. Raven Block II (From [9]).

In 2005, after a competitive source selection process, AeroVironment Inc. in Simi Valley, California, was chosen by the U.S. Army for their upgraded Raven, the B model. A Milestone C decision was approved in October 2005. The Raven B went through Initial Operational Test and Evaluation from May to June 2006 at Fort Bliss, Texas. Full Rate Production decision occurred in October of that same year. The Raven B Basis Of Issue Plan (BOIP) for Army acquisition objective was 2,182 systems. Current procurement objective is 2,079 systems. There are approximately 855 Raven B systems fielded to the Army and National Guard. Raven B is fielded to the Brigade Combat Teams (BCTs) with 15 systems each. In Operation Iraqi Freedom (OIF) there were 255 systems and 41 Raven B systems supporting Operation Enduring Freedom (OEF). U.S. Special Operations Command (USSOCOM), the U.S. Marine Corps, and U.S. Air Force also employ the Raven B [10].

In late 2006, the Army began fielding the Raven RQ-11B version. The RQ-11B, shown in Figure 7, is manufactured by AeroVironment. The RQ-11B system is an upgraded version of the battle-proven Raven A, which is no longer produced. It

is a lightweight system designed for rapid deployment and high mobility for both military and commercial applications. The Raven B is the most advanced Small Unmanned Aerial System (SUAS) deployed with U.S. armed forces [11].

Figure 7. Raven RQ-11B SUAV (From [12]).

In December 2009, the Raven B was upgraded to Digital Data Link (DDL), replacing its analog command link and video. Additional upgrades include digital/encrypted Full-Motion Video (FMV) and aircraft control, and future interoperability with Unmanned Ground Vehicles (UGV) and Unattended Ground Sensors (UGS) [10].

The Pathfinder Raven SUAV has become the first military useful man-portable SUAV to be produced in large quantities and represents an essential part in the fight against Terrorism.

B. ACQUISITION STRATEGY

1. Acquisition and Cost

The demand for the Raven RQ-11B has been such among combatant commanders that in November 2005, the Raven became the official U.S. Army SUAV, responding to a USSOCOM Operational Requirements Document (ORD). Full rate production began in 2006 and is expected to last until 2014. The initial buy was for 1,328 systems plus training and logistics support. The current Army objective for Raven acquisition is 2,182 systems, representing over 6,000 aerial vehicles owned by DoD. The latest order was received in February 2009, as the U.S. Army awarded AeroVironment an order worth $41.7 million for Raven SUAS, fulfilling requirements for Army, SOCOM and the USMC. Apart from the U.S. forces, Raven operators include the Italian, Dutch, Danish and Spanish forces. This year, the Army is planning to buy 704 more new Ravens at a price tag of $79.65 million. Similarly, the Navy and the Marine Corps are spending $55.4 million for 517 new Ravens. This is all included in the fiscal 2010 U.S. Department of Defense (DoD) proposed budget [13].

In February 2010, the U.S. Department of Defense awarded a $37.8 million contract to AeroVironment to design and develop advanced digital Ravens, retrofit kits and spare parts, and provide repair and training services to the U.S. Army and U.S. Marine Corps. The advanced digital Raven system offers higher communication security through signal encryption. The deliveries of the upgraded digital Ravens are scheduled to begin in the next 12 months [11].

Despite the enormous amounts of money spent by the DoD on a single unmanned aircraft, no one can deny that what makes the Raven so popular is its cost. The price tag for a single Raven aircraft is about $35,000, and the total system costs $250,000.

2. Training

Regardless of the different levels of autonomy encountered in the Raven UAV, its successful operation depends on a well trained operator. Army Raven B operators are either trained during unit fielding by the Program Manager of Unmanned Aerial Systems (PM-UAS)/vendor New Equipment Training Teams (NETT) or at the 2nd Battalion, 29th Infantry Regiment, 197th Infantry Brigade located at Fort Benning, Georgia. This facility includes institutional training, Mobile Training Teams (MTT). The training for the Raven B is divided into three programs of instruction: the operator's course, one system remote video terminal (OSVRT) course, and the Master Trainer's course. Fort Benning conducts 24 classes per year with 12 students per class, turning out between 350 and 500 Raven operators per year. Their Mobile Training Teams also contribute a significant number of new operators each year [14]. From Figure 8, it can be seen two soldiers performing preflight checks on the Raven UAV.

Figure 8. Preflight checks of the Raven UAV (From [15]).

USSOCOM also conducts institutional operator training for USSOCOM personnel at Eglin Air Force Base, Florida, and San Clemente Island, California. PM-UAS, Fort Benning and USSOCOM all use the current United States Army Aviation Center of Excellence (USAACE) Program of Instruction (POI)/Training Support Package (TSP). The operator course is 10 training days and the Master Trainer course is five training days. The U.S. Army Aviation Center of Excellence at Fort Rucker and the Maneuver Center of Excellence (MCE) at Fort Benning are reviewing the feasibility of master trainers' ability to train and certify operators at home station [10].

The great capabilities offered to the commanders on the field by the Raven B have increased the demand for this asset. As a result, the need for more operators becomes critical. Fortunately, the Army is developing a formalized UAS training strategy that will support the breadth and depth of UAS operations [14].

C. SYSTEM CHARACTERISTICS AND COMPONENTS

1. System Composition

The Raven B system includes three aircraft, a ground control unit (GCU), a remote video terminal unit, spare batteries, a charger, and support equipment. It also has an autoland feature and an interoperable system interface unit. The UAV is fully equipped with an automatic launch and recovery (ALR) system, which aids in automatic safe landing during communication failure with the GCU [11]. Table 1 shows the list of components and their respective quantities included in one Raven system. The pictures of each individual component in a Raven system are shown in Figure 9.

Table 1. Raven System Composition (From [16]).

Component	Quantity
Aircraft	2-4
EO Camera Payload Nose – Front & Side Look	1
IR Camera Payload Nose –Front Look	1
IR Camera Payload Nose –Side Look	1
GCU	1
Remote Video Terminal	0-1

Figure 9. RAVEN RQ-11B SYSTEM (From [16]).

As shown in Figure 10, each individual Raven SUAV consists of the following parts:

- Nose cone - encloses Infrared (IR) and Electro-Optical (EO) cameras
- Fuselage - houses the electric motor, propeller, pitot-static tubing, payload electronics, and a rechargeable lithium-ion battery
- Wing – divided in three sections: left/right wing tips and one center wing
- Tailboom – connects the rudder and stabilizer to the fuselage
- Stabilizer

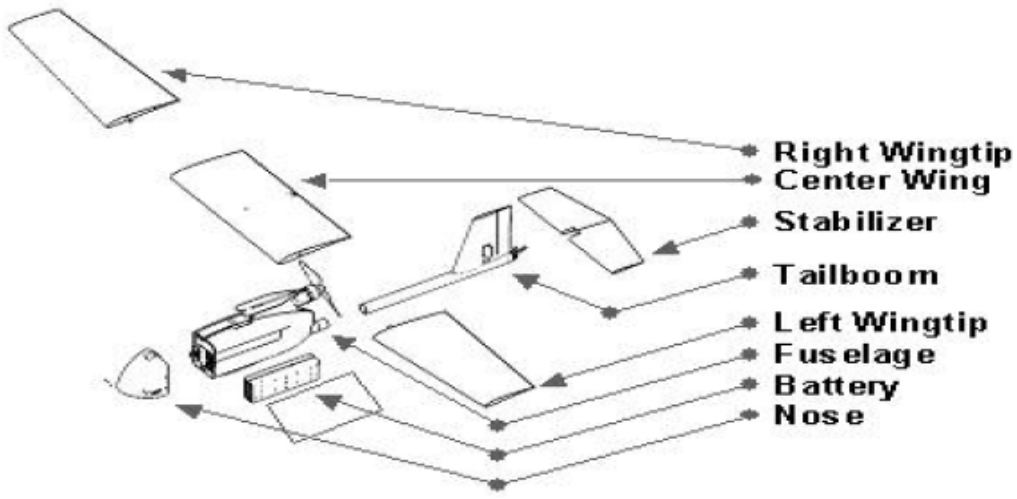

Figure 10. Raven RQ-11B Parts Breakdown (From [16]).

2. Performance

The RQ-11B UAV can fly at a maximum altitude of 500ft (152m). The maximum cruising speed of the aircraft varies between 32km/h and 81km/h. The range and service ceiling of the aircraft are 10km and 4,500m, respectively. Its maximum endurance is 90min. The aircraft weighs around 4.2lb (1.9kg). It has a wingspan of 4.5ft and reaches 36 inches in length [11]. The performance characteristics of the Raven UAV can be seen in Table 2.

Parameter	Characteristic
Wingspan	55 inches
Length	36 inches
Structure	modular, Kevlar™ composite
Weight (with payload)	4.0 lbs
Payload Nose Weight	6.5 oz
Operating Altitude	150 to 1000 ft AGL
Nominal Low Altitude	100 ft
Cruise Speed	30 mph (13.5 m/s)
Range	10 km (LOS)
Climb Rate	900 ft/min @ 2000 ft AGL
Turn Rate (360°)	25 seconds
Motor	direct drive electric
Aircraft Batteries	$LiSO_2$ (single-use) Li-Ion (rechargeable)
Flight Duration	90 + min rechargeable 90 + min single-use
Launch	hand
Landing	commanded autoland deep stall
Navigation	P(y)-code GPS and electronic compass
Flight Control	manual or autonomous

Table 2. Raven Specifications (From [16]).

3. Payload

The Raven carries an Electro-Optical (EO) or Infrared (IR) payload which provides aerial observation, day or night, at line-of-sight ranges up to 10 kilometers (shown in Figure 11). Both cameras are located inside the nose cone and together weigh 6.6 ounces. The EO sensor converts light rays into electronic signals for capturing images, real-time data and videos. It had a front and side look camera. This data is then delivered to the ground control and remote viewing stations [6].

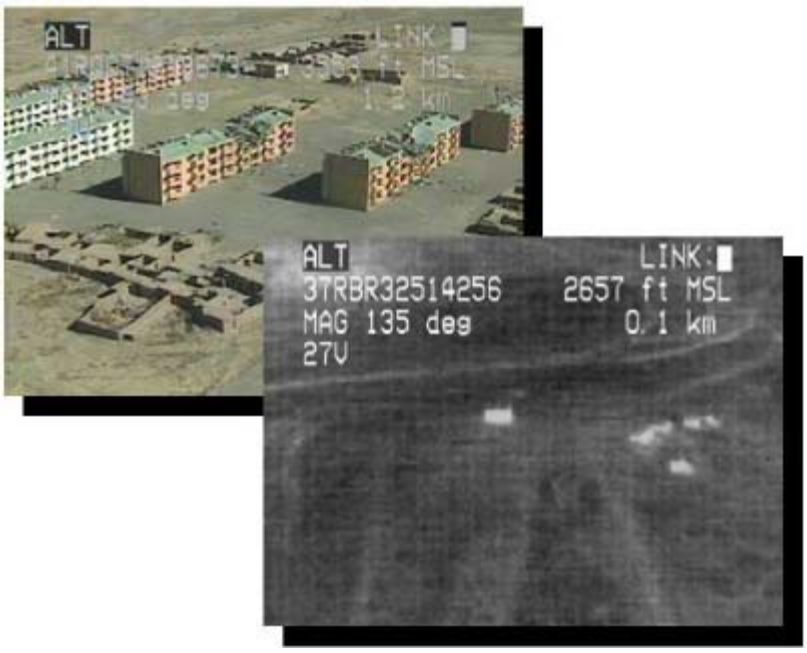

Figure 11. Day and Night Video Imagery (From [8]).

The IR payload has only a side look and includes a laser IR illuminator, which is visible with night vision goggles but not visible through the thermal imager in the IR payload. The EO payload is equipped with a fixed digital front camera capable of pan, tilt, and zoom functions [17].

4. Navigation

The RQ-11B can be controlled either manually from the ground control station or through the autonomous mode. The Raven B system provides fully automated take-off and landing even in adverse weather conditions using advanced avionics and a precision global positioning system (GPS) system [11].

5. Engine

The RQ-11B Raven is powered by a single Aveox 27/26/7-AV electric motor. The engine is manufactured by U.S.-based

Aveox. Each engine features an integrated starter or generators, flight surface actuation systems, integrated gearboxes, shafts, cooling fans and pumps [11].

6. Ground Control Unit

The Ground Control Unit (GCU) is a compact and lightweight system, which displays real-time videos or images captured by the vehicle's payload cameras [11].

The processing, retrieving and storing of the real-time data provided by the UAV is carried out at the GCU. It also plays back videos for target evaluation and alleviate retransmission of videos and meta data to the operations network [11].

The GCU can be operated as a remote video terminal (RVT) when implanted at remote location. It also enables the command centers to view and analyze the data. The ground control unit can be easily assembled or disassembled in just 2 minutes [11].

7. Portability

The Raven has the advantage that it can be easily transported in three small cases that can fit into a ruck sack. The wing is divided into three small sections which facilitates its transportation. It can be launched within minutes by hand and it lands by itself without requiring a landing gear or a landing strip.

D. SYSTEM LIMITATIONS

1. Battery Life

One of the constrictions encountered on this UAV is the limited amount of flight time it provides to the opera-

tor on a single mission. The Raven SUAV is a battery operated aircraft. Six lithium-ion (Li-ion) polymer cells make up the RQ-11B rechargeable battery pack. It has a fully charge voltage of 25.2VDC and a capacity of 4 Ampere hours (Ah). The battery can last from 60 to 90 minutes under normal flying conditions on a single mission. Additional factors that may affect the endurance of the aircraft are: altitude, wind currents, winds speeds, temperature, etc.

2. Altitude

The maximum flight altitude is 10,500ft; however, flying at that level may impact flight performance, primarily reduced climb rate and flight endurance [17].

The normal operating altitude is 150ft to 1,000ft above ground level (AGL). Operating above 500ft AGL reduces video sensor performance [17].

3. Wind Speed

The Raven UAV is designed to sustain wind speeds of up to 20 knots to include flying under blowing sand and dust. It could operate in winds higher than 20 Knots but with reduced mission capability and higher risk of damage during launch, landing, and recovery. Flying at that rate also implies reduction in flight endurance, since more battery power is consumed [17].

4. Temperature

Additionally, its system components have maximum operating temperature range of 50-degrees Celsius and a minimum of 29-degrees Celsius. However, operating under extreme low temperatures reduces the battery life of the UAV [17].

Without a doubt, the success of the Raven program is attributed to the well-thought aircraft design, which evolved around supporting that soldier and Marine on the ground. The performance characteristics described in this chapter has made the Raven SUAV the weapon choice for combatant commanders on the field, providing them with "over the hill" intelligence in direct support of their respective battalion's activities. Despite their limited flight endurance, Ravens continue to support Army and Marine Corps units in Iraq and Afghanistan. Indeed, more needs to be done with respect to extending flight endurance of the Raven RQ-11B SUAV. Only the application of the latest solar cell technology can greatly improve its performance and provide hours of uninterrupted route reconnaissance, battle damage assessment, force protection, convoy protection, surveillance, intelligence gathering, etc., without the need for retrieving the Raven every 90 minutes to replace its battery.

III. CIGS TFPV CELLS

A. INTRODUCTION

$CuInGaSe_2$ (CIGS) polycrystalline thin film photovoltaic cells are a realistic option for reaching the goal of low-cost, high efficiency power conversion from renewable energy sources [18].Equation Chapter (Next) Section 3

One of the great advantages offered by a CIGS TFPV cell is its efficiency, i.e., the ability to produce the greatest amount of electricity for a given illumination level. Research groups around the world have successfully reported a steady increase in efficiency of laboratory devices. For example, in March 2008, the National Renewable Energy Laboratory (NREL) reported an efficiency of 19.9%. Recently, the Centre for Solar Energy and Hydrogen Research in Germany reported a record of 20.1% efficiency in thin film CIGS cells [19].

Although much improvement in efficiency is seeing in laboratory devices, the manufacturing arena is slowly leveling the field. For example, Global Solar, the leading manufacturer of CIGS thin-film solar on a flexible substrate, has developed 10% and 13% efficient thin film cells. A single CIGS thin-film solar cell is shown in Figure 12.

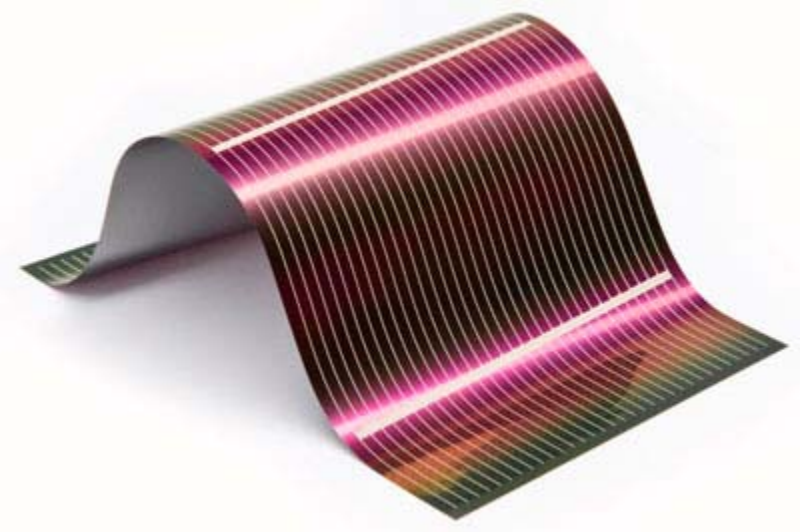

Figure 12. CIGS TFPV Cell (From [20]).

Other advantages of this type of cell include its flexibility and lightweight which make this type of photovoltaic (PV) cell suitable for a variety of applications such as the one included in this research. It is worth mentioning that our research was conducted using 13% efficiency CIGS TFPV cells from Global Solar.

B. SOLAR SPECTRUM AND SOLAR RADIATION

Solar radiation at the Earth's surface varies due to atmospheric effects, latitude and location, season of the year, and time of the day. Elements encountered in the atmosphere absorb the incident photons resulting from solar radiation. Gases like ozone, carbon dioxide, and water vapor absorb those photons with similar bond energy than those gases. Nonetheless, dust particles and aerosols have a greater impact on reducing the power from solar radiation. They not only absorb photons, they also produce scattering of light [21].

The solar spectrum is referenced through the Air Mass (AM), which quantifies the reduction in the power of light as it passes through the atmosphere. Outside the Earth's atmosphere the reference spectrum is (AM 0), which corresponds to a solar radiation with an intensity of approximately 1370 watts per square meter. This is considered the solar constant and it is the value at mean Earth-Sun distance at the top of the atmosphere [22]. This spectrum is normally used to predict the performance of solar cells expected to be used in space. At the surface of the Earth, on the other hand, the solar spectrum reference is (AM 1.5), which has a normalized solar radiation intensity of 1,000 Watts per square meter. From Figure 13, the different path lengths of irradiation can be observed. Air mass varies with location on the surface of the Earth.

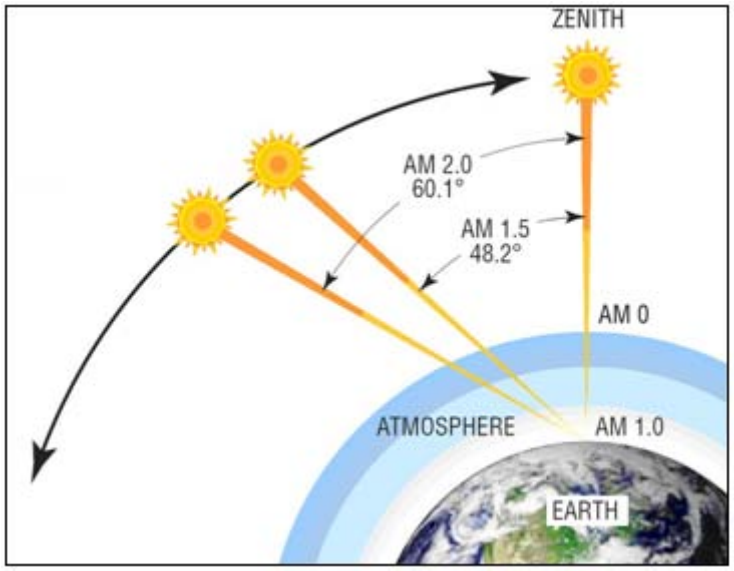

Figure 13. Air Mass (After [23]).

C. SOLAR CELLS

PV cells, commonly known as “Solar Cells,” come in a variety of materials and processes that can potentially satisfy the requirements for photovoltaic energy conversion, but in practice nearly all photovoltaic energy conversion uses semiconductor materials in the form of a *p-n* junction [21].

1. P-N Junctions

P-n junctions result from joining n-type and p-type semiconductor materials. The n-type region contains high electron concentration and the p-type high hole concentration. Thus, electrons diffuse from the n-type side to the p-type side, recombining with holes. Similarly, holes flow by diffusion from the p-type side to the n-type side. If the electrons and holes were not charged, this diffusion process would continue until the concentration of electrons and holes on the two sides were the same, as happens if two gasses come into contact with each other. However, in a p-n junction, when the electrons and holes move to the other side of the junction, they leave behind exposed charges, creating an electric field between the positive ion cores in the n-type material and negative ion cores in the p-type material. This region is called the "depletion region" since the electric field quickly sweeps free carriers out, hence the region is depleted of free carriers. A "built in" potential V_{bi} due to the electric field is formed at the junction [21].

2. Band Gap

The band gap of a semiconductor is the minimum energy required to free an electron from its orbit to become a mobile charge carrier and participate in conduction. To better understand the band structure of a semiconductor a band diagram is used to show the energy of the electrons as they move inside the semiconductor material. The valence band is the lower energy level of a semiconductor and the conduction band is where an electron is considered free. The band gap is the distance between the conduction band and valence band [21]. Figure 14 shows the band diagram of a p-n junction and how carriers are generated by an incident photon and separated by the built-in electric field of the depletion region. The Fermi level depicted in Figure 14 indicates the type of conducting material.

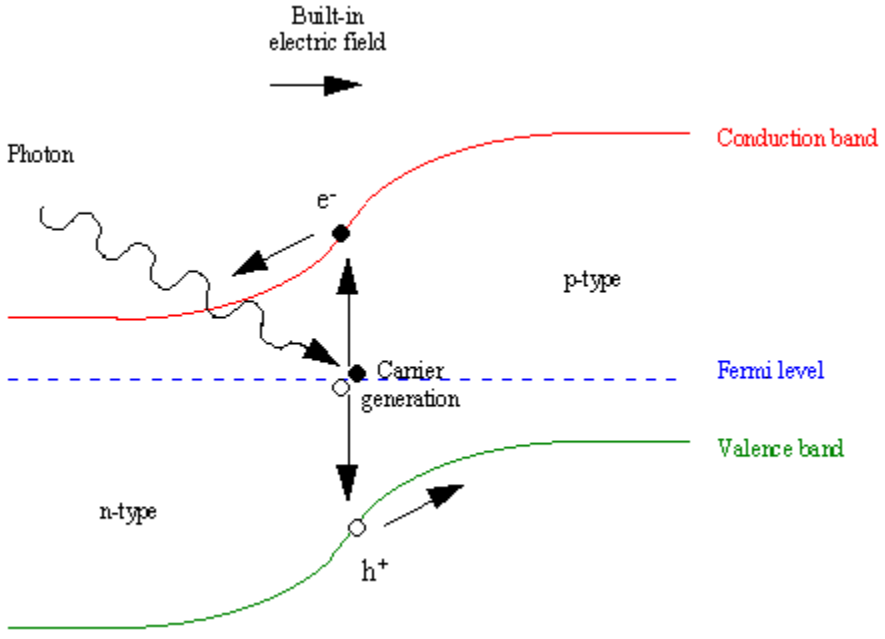

Figure 14. Band Gap Diagram (From [24]).

As the electron in the conduction band moves freely about the semiconductor and participates in conduction, the movement of an electron to the conduction band leaves behind an empty space for an electron. Another electron from a neighboring atom can move into this empty space; hence, leaving behind another space. This repeated movement of the space for an electron is called a "hole" and can be considered as the movement of a positively charged particle through the crystal structure. As a result, we observe movement of electrons in the conduction band and holes in the valence band. This movement of electrons and holes that participate in conduction are called "carriers" [21].

3. Photovoltaic Effect

Simply put, the photovoltaic effect is the transformation of radiation or solar energy into electrical energy. As shown in Figure 14, when light hits the surface of a solar cell (SC), incident photons are absorbed, creating electron hole pairs. This happens only if the photon has greater energy than the band gap of the semiconductor materials that conforms the SC. The p-n junction collects these carriers and separate electrons and holes through the built-in electric field of the depletion region, preventing recombination and creating voltage or a corresponding electric current [21].

4. Solar Cell Structure

A solar cell or photovoltaic cell is layered structure comprising different layers, such as antireflection, light absorbing material, metal electrical contact. The antireflection layer is made of an electrically conductive mate-

rial that permits light to pass to the absorber. The absorber is a layer of semiconductor material in the form of a p-n junction that absorbs the light photons necessary to generate electrons via the photovoltaic effect. This type of material absorbs wavelengths of solar light that reach the Earth's surface. Lastly, each solar cell must have a front and back metal contact which is where the device generates a voltage differential and electrical current, depending on the intensity of the light. The front electrical contact layer is in the form of a grid pattern to avoid shelf-shading. The cross sectional area of a solar cell is shown in Figure 15.

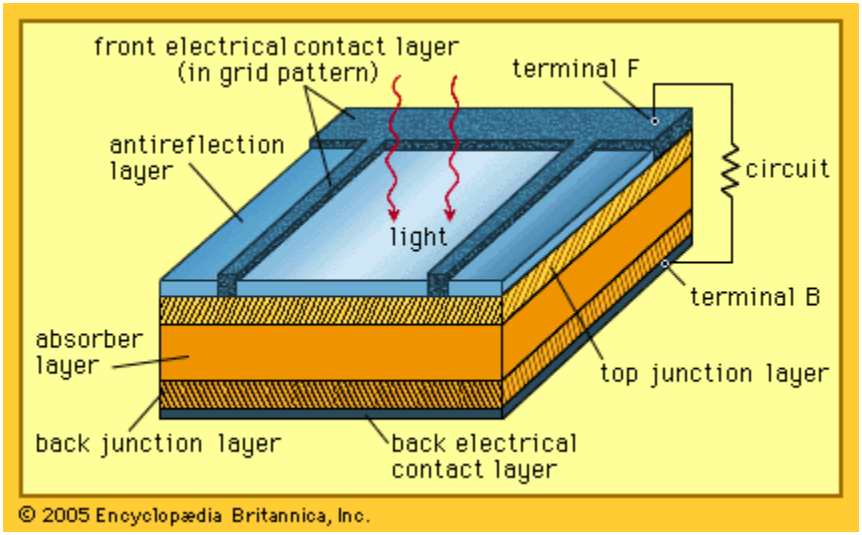

Figure 15. Solar Cell Structure (From [25]).

5. Thin-Film Photovoltaic Cells

When looking for a quick description of what a CIGS TFPV cells are, most search engines on the Internet would describe them as:

> CIGS belongs in the category of thin film solar cells (TFSC). The semiconductors used as absorber layer in TFPV exhibit direct band gaps allowing

the cells to be a few micrometers thin; hence, the term TFSC is used to refer to them. [26]

Thin-film photovoltaic cells are made of one or more thin layers of absorber or photovoltaic material on a substrate. It is this characteristic that makes these solar cells flexible and lightweight. TFPV cells are cheaper than thick-film solar cells because they are manufactured with a smaller amount of light absorbing materials. This leads to reduced processing costs from that of bulk materials, but at the same time, reduces the energy conversion efficiency of the cell. TFSC are usually categorized according to the light absorbing material used. The most common photovoltaic materials used are: Amorphous Silicon, Cadmium Telluride, Copper Indium Gallium Selenide. For the purpose of this research, we focused on CIGS TFPV cells, only [26].

Throughout the years, great achievements in energy conversion efficiencies for these types of cells have been made. In 2008, the National Renewable Energy Laboratory (NREL) reported a 19.9% efficiency which was by far the highest compared with those achieved by other thin film technologies such as Cadmium Telluride (CdTe) or amorphous silicon (a-Si) [27]. On 29 April 2010, scientists from the Centre for Solar Energy and Hydrogen Research based in Stuttgart, Germany reported a new record efficiency of 20.1% efficiency on a 0.5 square centimeter cell. They further claim that this efficiency obtained is for thin film cells in general and not only for CIGS [19]. It is important to note that these are lab-scale achievements and have not made their way into production. The industry of TFPV cells still displays lower energy conversion efficien-

cies of 10% and 13%. In the long-term however, thin-film technology is expected to overtake thick-film technology in terms of growth. It will go hand in hand with the worldwide demand for photovoltaic systems [20].

D. CIGS AND SILICON

CIGS TFPV cells differ from silicon TFPV cells in that their semiconductor material interface occurs between regions of dissimilar crystalline semiconductors with different band gaps. As mentioned before, CIGS TFPV cells are not as efficient as crystalline silicon solar cells but they are expected to be substantially cheaper due to the reduced amount of absorbing material used in its fabrication, which results in a much lower cost for material and fabrication. Being a direct band gap material, i.e., electrons in the semiconductor material can shift from the lowest energy state in the conduction band to the highest energy state in the valence band without a change in the crystal momentum, CIGS have very strong light absorption, and therefore, they can be made with a very thin active layer. Often 1-2μm of CIGS is enough to absorb most of the sunlight. The opposite occurs with silicon since greater thickness of crystalline silicon is required for the same absorption [26].

E. CIGS STRUCTURE

Most p-type CIGS TFPV cells are fabricated on glass, mylar or stainless steel substrates. Nevertheless, the most common substrate is soda-lime glass because it is electrically insulating, comparatively cheap, temperature stable and with a smooth surface. This substrate is coated using

physical vapor deposition (PVD) on one side with molybdenum (Mo) that serves as metal back contact. CIGS and ZnO form a hetero-junction, where CIGS is doped with p-type material and ZnO with the n-type material through the incorporation of aluminum (Al). It is this asymmetric doping that causes the space-charge region to extend much further into the CIGS than into the ZnO. Both materials are buffered by a thin layer of CdS using a wet chemical method called Chemical Bath Deposition (CBD). The main role of this buffer is to passivate the absorber surface and to provide suitable partnering material between CIGS and ZnO. The buffer layer is followed by a thin layer of highly resistive ZnO which protects the surface and evens out the potential. To minimize the absorption, the upper layers need to be minimized by increasing the band gap of ZnO and CdS (($E_{g,ZnO}$=3.2eV and $E_{g,CdS}$=2.4eV), respectively. The front contact consists of a transparent conducting oxide (TCO). TCO consists of heavily ZnO doped with aluminum (Al). The front contact is used for current collection [28]. The basic structure of a $CuInGaSe_2$ thin-film solar cell is depicted in Figure 16.

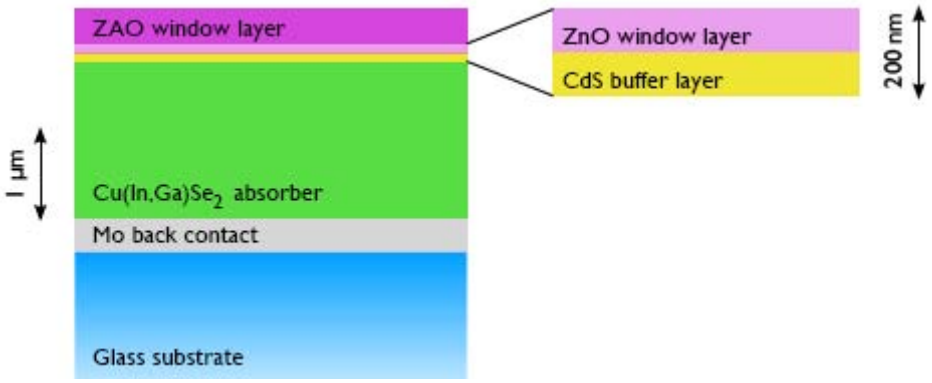

Figure 16. CIGS Cell Structure (After[28]).

F. CIGS DEGRADATION

To date, the level of understanding of performance degradation among different TFPV cells is still inadequate. Oxygen and temperature seem to be a major cause of degradation. Recent studies conducted by the National Renewable Energy Laboratory on thin-film CdS/CdTe solar cells have concluded that oxygen affects the cell performance by suppressing the interdifussion at the junctions.

> Without the presence of oxygen, the interdifussion can be substantial, resulting in fully consumed CdS regions, which have same effects as pinholes, and high Te concentration $CdS_{1x}Te_x$ regions, which have a lower bandgap than CdS. This leads to reduced V_{oc} and J_{sc} for the CdS/CdTe solar cell. [29]

It was then determined that oxygen impurity in CBD-CdS films is therefore proposed to be the main cause for the different solar performance using CBD-CdS and non-CBD-CdS as window layers [29].

Another study conducted by NREL scientists on CdTe devices determined that at temperatures from 90-degrees Celsius and 120-degrees Celsius, degradation is dominated by Cu diffusion from the back contact towards the electrical junction. At lower temperatures degradation is not known. Nonetheless, these findings greatly affect the encapsulation process and the need to find materials that can cure at room temperatures [30].

Nevertheless, the thickness of the light absorbing materials used in the fabrication of TFPV cells can also degrade its performance. As seen in Table 3, using semiconductor materials with less than 1μm thickness can greatly reduce the energy conversion efficiency [30].

Table 3. Summaries Thin Cells Efficiencies (From [30]).

t (μm)	V_{OC} (V)	J_{SC} (mA/cm^2)	FF (%)	Efficiency (%)
1.0 CIGS	0.676	31.96	79.47	17.16 NREL
0.75 CIGS	0.652	26.0	74.0	12.5
0.40 CIGS	0.565	21.3	75.7	9.1
0.47 CIGS	0.576	26.8	64.2	9.9 EPV
1. CIGSS Module	25.26	2.66	69.2	12.8 Shell Solar
0.87 CdTe	0.772	22.0	69.7	11.8 U. of Toledo

The introduction of TFPV cells technology has revolutionized the industry of solar energy. To date, CIGS are being incorporated to many applications due its flexibility, low cost, and lightweight benefits. Our research is based on the use of CIGS TFPV cells along with other power electronic devices that would generate enough power to extend the flight time of the Raven RQ-11B, which are described in the next chapter.

IV. POWER INTEGRATION

As explained in Chapter III, the amount of power provided by a solar cell varies throughout the day and is based on external factors such as temperature, irradiance, angle of incidence, etc. For this reason, we first look into other electronic components that could overcome this effect and help us achieve the desired power levels. Equation Chapter (Next) Section 4

A. DC-DC POWER CONVERTER

As it will be described later in Chapter V, the surface area available for this project allowed a total of forty solar cells connected in series to serve as an additional power source. Given the fact that each CIGS TFPV cell had maximum output voltage of 0.5VDC and an efficiency of 13%, our initial calculations estimated a maximum output voltage from the solar panel of 17VDC, as seen in equations 4.1 and 4.2.

$$V_{panel} = V_{cell} \times N_{cells} - \left(V_{cell} \times E_{ff}\right) \tag{4.1}$$

$$V_{panel} = 0.5 \times 40 - \left(0.5 \times 0.13\right) = 17.40\,VDC \tag{4.2}$$

In equation 4.1, V_{panel} represents the total voltage of the solar panel, V_{cell} is the voltage given by a single CIGS solar cell, N_{cell} represents the number of solar cells, and E_{ff} is the efficiency of the solar cells obtained for this project.

Therefore, it was imperative to look into a boost (step-up) DC-DC power converter to get a higher voltage that would enable us to charge a 25.2VDC Lithium-ion (Li-ion) Raven battery.

Step-Up (Boost) converters are power converters designed to provide an output voltage greater than the input voltage. Their basic circuitry consists of at least two semiconductor switches (a diode and a transistor) and at least one energy storage element [31]. The basic circuitry of a boost converter is shown in Figure 15.

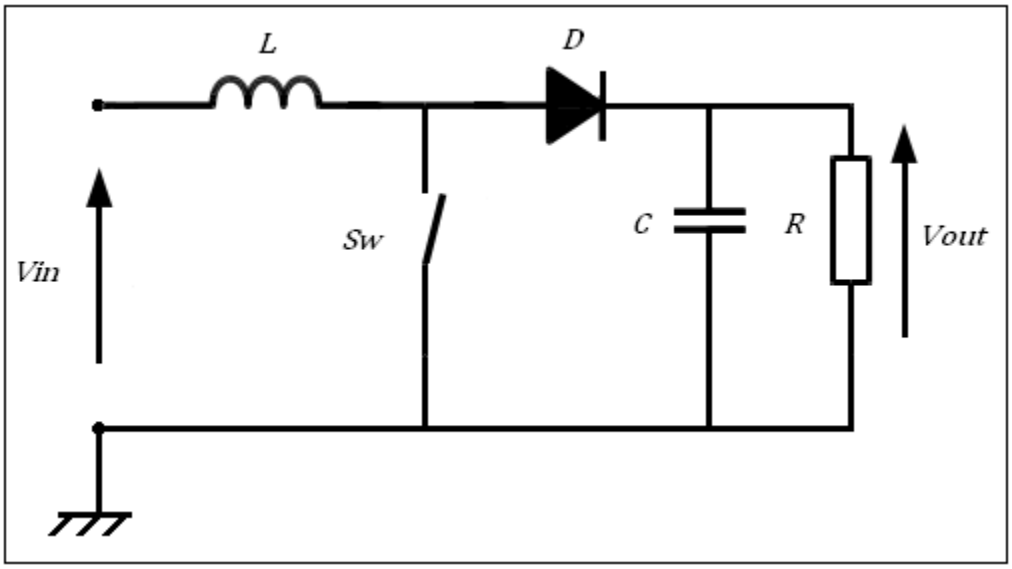

Figure 17. Boost Converter Schematic (After [31]).

This type of converter operates in the following manner: when the transistor switch is on, the inductor receives energy from the DC source and the diode is reverse biased, preventing the capacitor from discharging. When the switch is off, the inductor current is forced to flow through the diode and the load. The output voltage of the boost converters is derived from the volt-second balance in

the inductor. With a duty ratio D of the switch, the output voltage V_{out} is given by equations 4.3 and 4.4, where t_{on} is the time when the switch is on, t_{off} is the time when the switch is off, and V_{in} is the input voltage:

$$D = \frac{t_{on}}{t_{on} + t_{off}} \tag{4.3}$$

$$V_{out} = \frac{V_{in}}{1 - D} \tag{4.4}$$

Thus, for all values of D less than 1, the output voltage is always greater than the input voltage. The capacitor needs to be large to maintain a constant output voltage [32].

High efficiency in a DC-DC power converter is a necessity. Ideally, we would like to have 100% efficiency; in practice, power converters have efficiencies between 70% and 95%. For this research, we were able to acquire a boost converter that had an efficiency of 96% to 98%.

B. MAXIMUM POWER POINT TRACKER

A more suitable component used in photovoltaic applications is the Maximum Power Point Tracker (MPPT). An MPPT is nothing more than a fully electronic system that varies the electrical operating point of the solar panel so that it can deliver maximum available power. To extract the maximum power from the source, the MPPT matches the resistance of the load to obtain a voltage from the source that

is suitable for the load. This operation agrees with the basis of the Maximum Power Transfer Theorem, which states that the maximum power is transferred from the source to the load when the resistance of the source is equal to the resistance of the load. It connects between the solar module and the discharged battery. It is a system that calculates the voltage at which the PV module is able to produce maximum power, regardless of the present battery voltage. Additionally, the MPPT includes a DC-DC converter which converts the calculated voltage at maximum power from the PV module to battery voltage; hence, eliminating the need for a separate power converter [33].

The charge current produced by the solar module can be calculated using equation 4.5:

$$I_{charge} = \frac{V_{sp}}{V_{batt}} \times I_{sp} \tag{4.5}$$

In equation 4.5, V_{sp} and I_{sp} are the calculated voltage and current of the solar panel at maximum power. V_{batt} is the voltage of the discharged battery [33].

C. BALANCER CHARGER

Dealing with Li-Ion batteries, which will be described in the next section, requires extreme caution. Electrochemical reactions may occur when over-charging and over-discharging Li-Ion batteries. These reactions can decrease the life of the cell as well as present a safety hazard. To minimize this effect, manufacturers have placed maximum and minimum voltage limits on individual Li-ion cells. Typical values are 4.0V to 4.2V and 2.5V to 3.0V for the maximum and minimum voltages, respectively. Nevertheless,

due to the variations in cell manufacturing processes and raw materials, it is necessary to control the voltages of the individual Li-ion cells within the Li-ion battery pack to avoid cell to cell imbalances [34].

A balancer charger is the electronic component designed to control the voltages of the individual cells in a Li-ion battery. Balancer chargers are built with different charge control strategies. Some monitor the battery voltage level, some monitor the cell voltage level, and others manage the cell voltage levels through dissipative and non-dissipated components such as resistors and capacitors.

For the purpose of this research, we concentrated our efforts in locating a balancer charger that would be light in weight and small in size compared to others in the market.

D. LITHIUM-ION BATTERIES

Since 1991, lithium-ion rechargeable batteries have been commercialized all over the world and have become a fastest growing system due to their high-energy density and lightweight. The Sony Corporation was the first one to put this product out on the market and most of their applications are now seeing in notebook computers, cell phones, and medical devices [35].

Lithium-ion batteries are preferred for their high-energy density (Wh/Kg), which refers to the amount of energy they can hold. The higher the energy density, the longer the runtime will be. They have twice the energy density and three times the voltage per cell compared to standard Nickel Cadmium (Ni-Cd) batteries [35].

Another advantage that makes these batteries so popular is the low maintenance needed. Most Ni-Cd batteries require being discharged 1V per cell periodically to prevent crystalline formation and to prolong their lifetime. This is normally caused by memory.

> Ni-Cd batteries have a cyclic memory which means that it remembers how much energy was drawn on preceding discharges. On a longer schedule discharge the battery voltage would drop rapidly and it would lose power. [35]

Lithium-ion batteries have also a lower self-discharge rate than other type of chemical batteries. When not being used or in storage, they slowly discharge. Li-ion batteries can discharge at a rate of 5% per month or lower compared to other Nickel based batteries that have a self-discharge rate of 10%-30% [36].

On the other hand, Li-ion batteries have certain drawbacks. For once, they require a protection circuit to limit the peak voltage of each cell while charging and prevent the cell voltage from going too low on discharge. However, this protection circuit causes problems after a long storage period. Isidor Buchmann, president of Cadex, Inc., states:

> If the battery is left discharged after use, the self-discharge will further drain the pack and eventually drop the protection circuit at about 2.5 volts per cell. At this point, the charger will no longer recognize the pack and the pack appears dead. [35]

In this chapter, we described the additional electronic components that would provide the best possible output power from our solar panel (SP). In the next chapter, we show how we put everything together, every step of the way.

V. DESIGN AND ASSEMBLY

After reviewing the history of the Raven SUAV program and its performance characteristics, understanding how CIGS TFPV cells work, and describing additional electronic components needed for this research, it was time to configure the Raven RQ-11B with PV cells in order to complement, if not, substitute the aircraft’s battery power, and therefore extend its flight time.Equation Chapter (Next) Section 5

A. WING MODIFICATION AND CONSTRUCTION

Our initial goal was to implement this idea over the original wings of the Raven SUAV. Nevertheless, our sponsors insisted us that we apply our concept on an extended wing which was designed and manufactured by mechanical engineers from the Composites Laboratory at the Naval Air Warfare Station in China Lake, California. Their intent was to increase the lift in order to add more electronics to the UAV. This idea turned out to be ideal since, at the same time, it gave us more flexibility to find the best design possible for our solar cells.

It was important to consider that the smaller the cell the less current that was going to put out. By having a larger area, we felt no need to make the cells too small which reduced the amount of labor involved in making the connections.

This modified wing was 40cm longer in the center section of the wing compared to the original. The wing tips had exactly the same dimensions as in the original wing tips. The dimensions of the wing are described in Table 4.

Table 4. Raven RQ-11B Wing Dimensions.

	Length	Width	Area
Center Wing	43.8cm	20.5cm	897.9sqcm
Right Wing	43cm	20.5cm/13.5cm	731sqcm
Left Wing	43cm	20.5cm/13.5cm	731sqcm

Figures 18 and 19 are picture representations of the original and modified Raven Wings. The shaded areas in Figure 19 represent the two extended areas designed which gave us more area to place more solar cells.

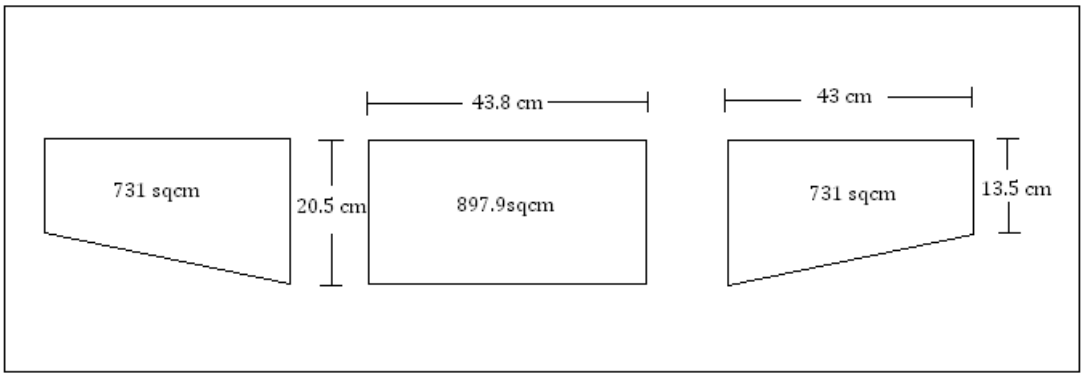

Figure 18. Raven SUAV Wing Dimensions.

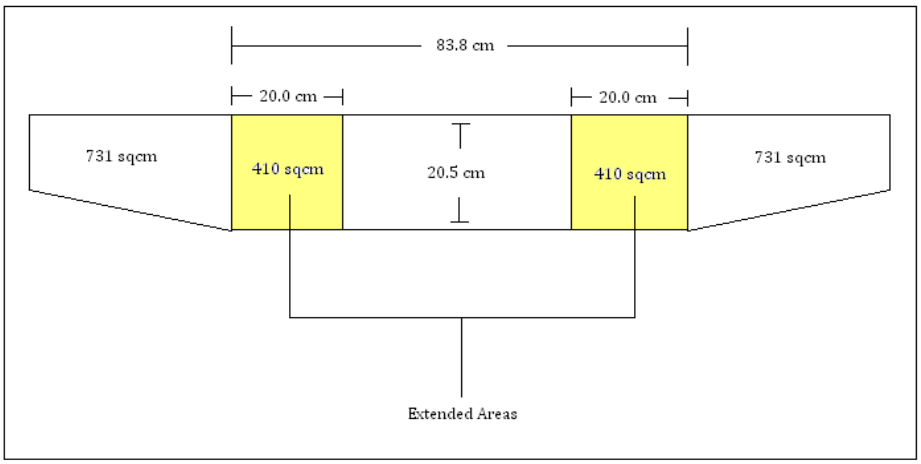

Figure 19. Modified Wing Dimensions.

Although the modification of the new wing was an advantage in regards to area available for solar absorption, it was manufactured as one big solid section which defeated its portability benefit. The difference in dimensions between the modified and original wings is shown in Figure 20.

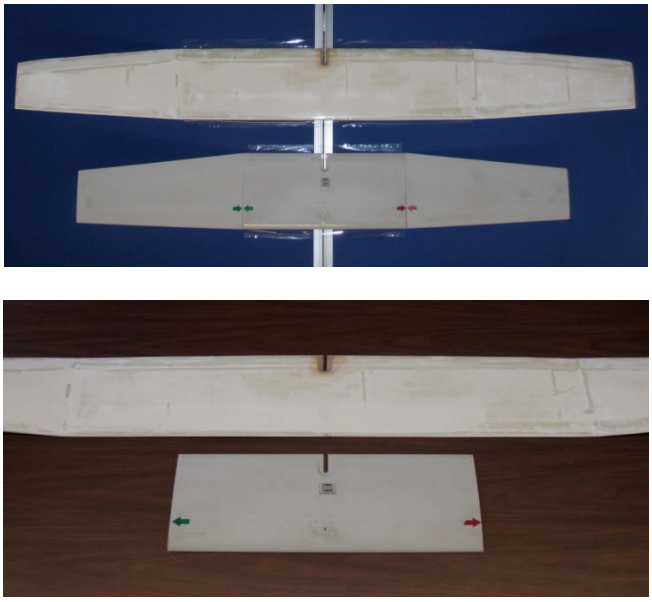

Figure 20. Original vs. Modified Raven Wings.

The original wing of the Raven RQ-11B comes in three separate sections, which is intentionally done to quickly disassemble the Raven UAV and place it inside a ruck sack to facilitate its transport.

The construction of the wing took several weeks to complete. However, it was critical to have a product with very similar characteristics as the original wings. The customized wing was made up of foam and fiberglass, exactly the same materials used on the original wings.

First, tooling was required to cast the foam. The two pieces that formed the cast for the foam are shown in Figure 21.

Figure 21. Tooling to Cast the Foam (From [37]).

Second, both pieces of tooling were clamped together to form a mold. After the mold was constructed, it was necessary to pour the liquid foam through the cavity, as shown in Figure 22.

Figure 22. Cast Clamped to Pour Foam (From [37]).

Once the foam core was made, as seen in Figure 23, it was removed from the mold and was then wrapped with fiber glass.

Figure 23. Foam Core (From [37]).

The final product is seen in Figure 24, next to the original Raven wings. Two modified wings were given to prove this concept.

Figure 24. Final Modified Wing.

B. SOLAR PANEL DESIGN

The next step was to come up with the best arrangement of solar cells that would give us the most output power, and at the same time, the least amount of cuts and connections possible. This was necessary to minimize the labor and the amount of handling involved.

1. Area vs. Power

A critical step in the design of the solar panel depended on the amount of energy provided from the sun. With the modified wing on hand and the information provided in Chapter III, we calculated the power per square centimeter that we expected to obtain from the solar panel.

Knowing that the standard AM1.5G spectrum has been normalized to give an intensity of 1KW/m^2, or 0.1W/cm^2 and that the area of our modified wing had a total surface area of 3,180cm^2, we obtained an input power P_{in} from the sun of 318 W. The CIGS TFPV cells had an output efficiency of 13%; therefore, we knew that our prospect solar panel would give us approximately 42W of output power $P_{Expected}$ (See equations 5.1 and 5.2). Nevertheless, it was necessary to consider that by leaving space in between cells and depending on daylight conditions, our output power would be somewhat lower than projected.

$$P_{in} = 0.1W/cm^2 * 3{,}180cm^2 = 318W \quad (5.1)$$

$$P_{Expected} = 318W * 0.13 = 41.8W \quad (5.2)$$

2. Solar Cell Arrangement

Given the surface area of the modified wing, there were many possible solutions to achieve maximum output power from a solar panel. However, after trying different designs, we opted for one that would give us the least amount of cuts, less number of solder connections, and the greater amount of solar cell area.

Global Solar Energy, our provider of CIGS TFPV cells, manufactures thin-film CIGS in strings of 18 cells connected in series, as seen in Figure 25. Each solar cell had 21cm in length and 10cm in width.

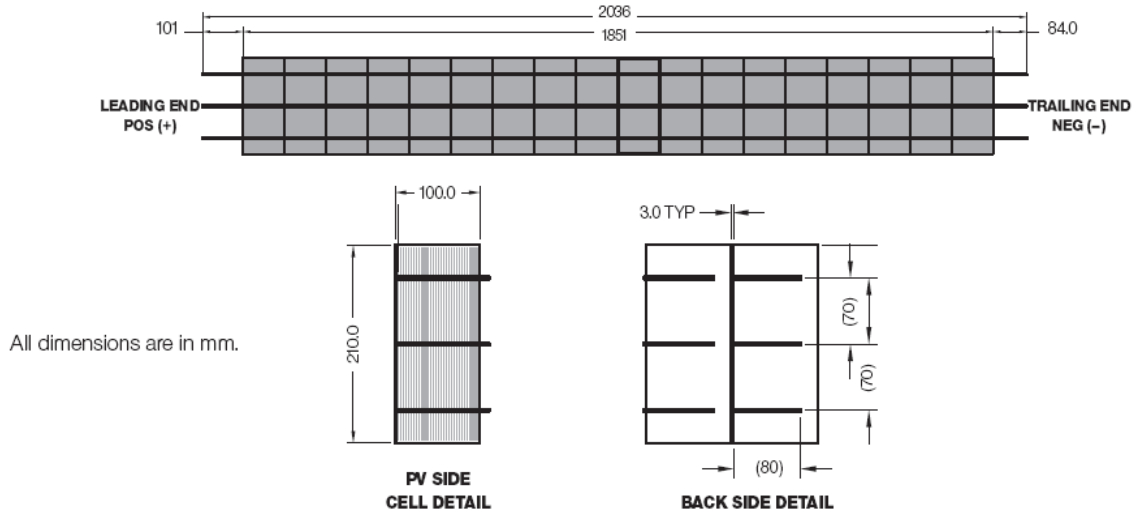

Figure 25. CIGS TFPV Cells from Global Solar (From [38]).

As mentioned earlier, it was not in our interest to make the cells too small. First, by reducing the area of each cell, we would be drastically reducing the amount of current. Perhaps, the benefit of making the cells small and connecting them in series is that we could have increased the amount of output voltage coming from the panel; however, by doing that we would have been reducing the total output current since it will always take the value of the smallest area of the solar cell on the panel. Therefore, it would have also reduced the power.

Another thing to consider was to cut the cells along the length of the string to minimize the number of solder connections that we would have to make between cells. On the other hand, cutting the cells across the width of the string was difficult because the center busses that ran across the cell were harder to cut and would short out the cell due to the pressure applied when cutting it.

With these considerations in mind, we proceeded to mount a total of 40 solar cells onto the surface area of the wing. Twenty-four cells measuring 6.3cm in width and 10cm in length were placed on the center section, covering an area of 1,512cm^2.

The layout for the wing tips was a bit challenging to make due to their trapezoidal shape. Also, it was necessary to take into account that while the aircraft would be flying and turning to either side, one of the wing tips would not be facing the sun directly; thus, the current for the entire panel would depend on the solar cells facing away from the sun. To minimize this effect, we made the area of the wing tip cells bigger compared to the cells on the center section. Regardless of their shape, we wanted the area of these cells not to go below 75cm^2. In the end, we covered an area of 383.28cm^2 in each wing tip, which gave us an overall solar cell area of 2,278cm^2. The final layout of the solar panel with the dimensions of each solar cell is depicted in Figure 26.

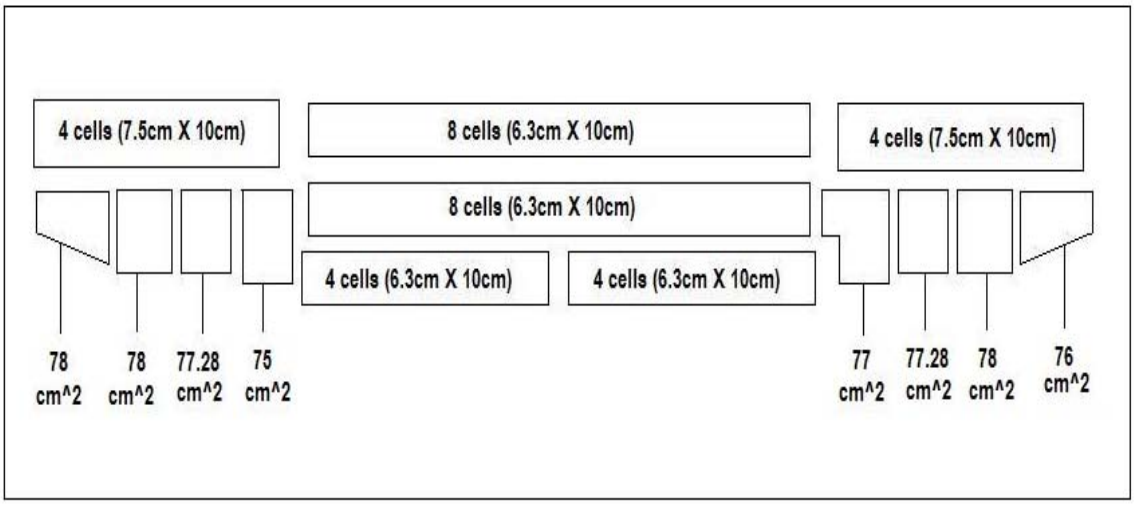

Figure 26. Solar Cell Arrangement.

After determining this new area of the wing that will be covered with solar cells, we went back to re-calculate the expected power $P_{Expected}$ that would be produced by our solar panel, using the same equations as in section 5A. The calculated expected power is seen in equations 5.3 and 5.4.

$$P_{in} = 0.1W/cm^2 * 2,279cm^2 = 228W \quad (5.3)$$

$$P_{Expected} = 228W * 0.13 = 29.64W \quad (5.4)$$

This time, we expected our solar panel to produce almost 30W of power, i.e., 12W lower than the 42W that we calculated using the entire area of the modified wing. Of course, this output power would be accurate only if we were under AM1.5G irradiance conditions.

C. CUTTING AND HANDLING OF SOLAR CELLS

1. Handling

Dealing with thin-film photovoltaic cells was not an easy task; especially, when the cells were not encapsulated. We decided to purchase CIGS cells without encapsulation to facilitate the cutting and to reduce the overall weight of the cells. Extra care needed to be taken when handling bare cells. For instance, we wore clean gloves to avoid adhesion-impact of moisture and oil from our hands. We also had to be extremely careful of not bending the string structure to avoid stress on the ribbon-cell bonds.

Normally, an encapsulated cell will have a thick lamination surrounding the cell which weighs 0.7-Oz compared to

0.2-Oz, which accounts for the weight of a single bare cell. Nevertheless, when a solar cell is not laminated, it runs the risk of degrading due to exposure to oxygen, humidity, and heat, as it was explained in Chapter III. Also, there is a good chance of damaging the cell due to accidental folding and bending of the cell.

For this reason, the manufacturer shipped its product in a hermetically sealed box. The minimum purchase order consisted of 50 strings of 18 cells each. Each cell's dimensions consisted of 21cm by 10cm. For our project we only needed one string which equaled a total of 18 cells.

To remove the strings from the box it was necessary to obtain a vacuum sealer to extract all the oxygen that leaks inside the box after removing the strings. This was done to prevent the rest of the cells from degrading. Additionally, we inserted nitrogen gas to eliminate any residual of oxygen.

After the cells were removed, it was necessary to place them in a sealed container or bag until they were ready to be worked on or connected.

2. Cutting

Cutting the cells was difficult and required some skill; thus, it was necessary to come up with the arrangement that would give us the least amount of cuts possible. Finding the right cutting tool was also a must. We tested several tools such as scissors, paper cutters, knives, etc., but every time we cut the cell we noticed that the mechanical movement of the tool created enough pressure on the anode side against the cathode side of the cell that

ended up shorting the cell out. We concluded that nothing worked better than a regular clean razor blade. In Figure 27, it can be seen our cutting technique on a bare CIGS solar cell.

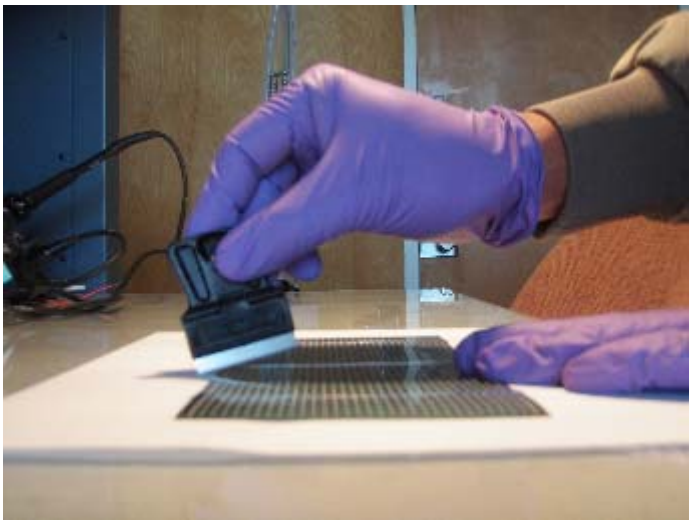

Figure 27. Cutting CIGS Solar Cell.

Without a doubt, the most difficult part about cutting the cells was cutting over the center conductor which was thicker compared to the cell grid. In order to avoid this obstacle, we peeled off the conductor before we made any cuts.

It is worth mentioning that every solar cell was tested for voltage and current under a halogen lamp to ensure that it was not shorted out and that it continue to maintain its functionality.

D. LAMINATION AND ENCAPSULATION

Before the cells were mounted and connected, they needed to be protected. Different types of plastic films were tested to determine its strength, transparency, adhesiveness, and durability. Strength in a plastic was needed

to sustain different weather conditions, high temperatures, as well as, tears or punctures. Transparency in a plastic was as important since it needed to allow the sunlight to go through without reflection. Adhesiveness was critical since it was necessary to hold the cells in place against the airframe of the wing of the Raven UAV. Finally, it was important to find a durable plastic material that would last a long time without changing its properties, i.e., discoloration or de-lamination.

We knew that Global Solar Energy, the manufacturer, uses some type of adhesive and moisture barrier for the lamination process, as seen in Figure 28, but using those materials increased the weight of the cell dramatically which was not convenient for our project.

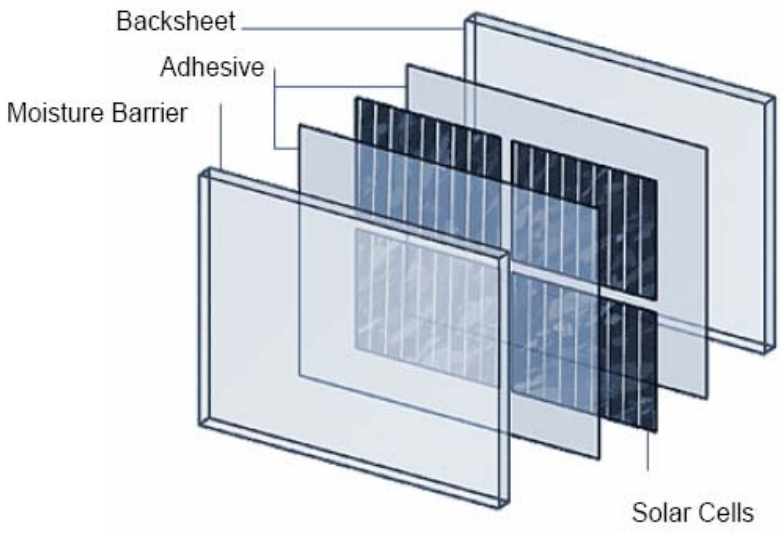

Figure 28. CIGS Module Cross-Section (From [38]).

After trying many different products in the market, the decision was made to acquire a clear, self-adhering protective film used on all types of carpeting. This plas-

tic film is a special blend of polyethylene and it coincided with all of our requirements that we had previously listed. The type of carpet protection film that we used is shown in Figure 29.

Figure 29. Carpet Protection Film (From [39]).

We laminated each solar cell individually. Although, tedious and lengthy, we found this method to be the best solution to avoid air gaps between the cell and the film and to prevent creases on the film.

Each solar cell was tested for voltage and current under a halogen lamp before and after lamination to ensure that no significant changes were present. For the most part, in all the tests, an increase of 1mA in current was observed after a single layer of plastic, since once the plastic was adhered to the cell it improved the absorption of light. The lamination process of a bare CIGS cell with carpet protection film is shown in Figure 30.

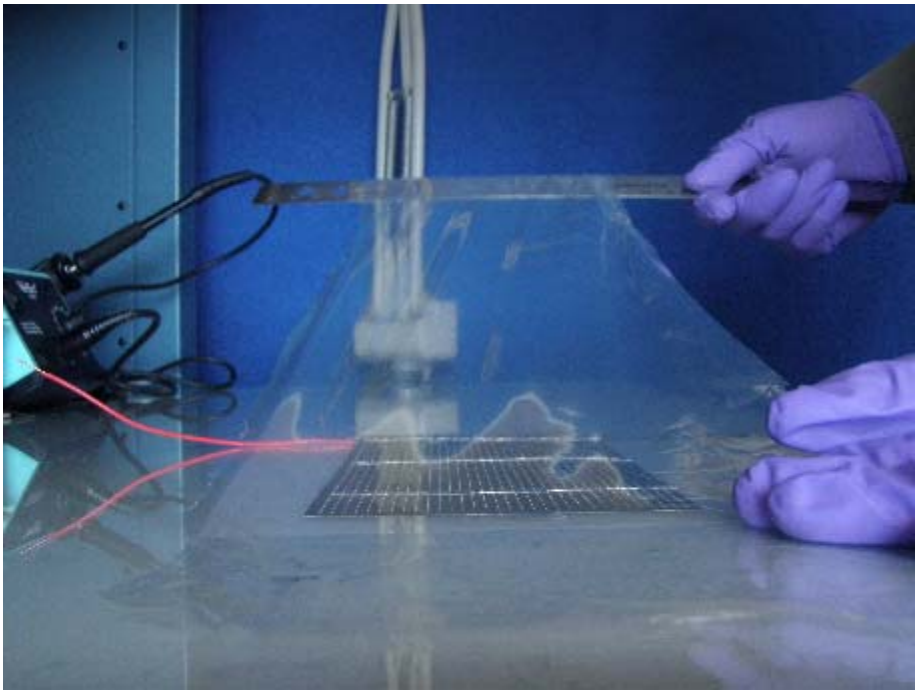

Figure 30. CIGS Cell Lamination.

Our sponsors did not allow us to make any permanent changes/additions to the wing; thus, we could not glue every solar cell to the wing. Instead, a second layer of carpet protection film was necessary to secure the whole arrangement against the wing.

E. WIRING AND CONNECTIONS

By cutting the majority of the cells along the length of the string, we avoided doing too many connections. The only connections left were in the wing tips and the connections coming from the panel to connect to the rest of the circuitry.

There were a few things to consider before connecting the solar cells. First, we were not sure about what type wire or conductor we needed to use. On one hand, we knew that the surface area of the modified wing would give us

approximately 40W of power and since our cells connected in series put out a voltage of 20V, we expected a maximum of 2A of current to flow through the wiring of the solar panel. Therefore, we had the option to choose a solid round wire anywhere from gauge 26AWG to 18AWG. However, a round conductor would have impacted adversely the air flow around the wing during flight due to its bulkiness. Another factor was its weight. Adding round solid wires would have increased the weight since the insulation of the wires also takes part into the equation.

We decided to use the same material used in the manufacturing process that came with the string of cells. Global Solar Energy uses 0.10mm X 25mm of tinned Copper (Cu) flat material that did not required lead tinning. Unfortunately, the number of flat conductors that we were able to obtain was not enough to complete the entire solar panel connection. Hence, we needed to use an alternative type of material but with similar characteristics as the pre-fabricated buss material. Cu conductor tape turned out to be the best solution for this situation. Cu conductor tape is flat and has the ability to adhere to any surface firmly. Additionally, its adhesive material is conductive which eliminates the use of soldering or any other methods to establish connectivity. Nonetheless, we decided to use solder to ensure the connections would not come apart while the UAV was flying. Figure 31 shows Cu conductor tape that we purchased for our project.

Figure 31. Copper Conductor Tape.

Another issue was deciding on whether it was safe to use solder or not. Our concern was damaging the cells due to excessive heat. An alternative solution was to use a new product called “Wire Glue.” This product is used for low voltage electrical connections and utilizes advanced micro-carbon technology. The manufacturer affirmed that Wire Glue was developed with epoxies and other adhesive systems with unsurpassed durability and strength [40]. Initially, the product adhered strongly to the other metals and its electrical connectivity performed as advertised. However, using Wire Glue was messy and the whole process turned out to be lengthy. As a result, we chose to use tin/lead solder, instead, heating the soldering iron to 370 degrees Celsius. From Figure 32, it can be seen a test conducted while gluing a solid wire to the buss of a solar cell.

Figure 32. Wire Glue Used on Solar Cell.

Finally, with the cells arranged on the wing, we looked at different ways to connect them in series. It was essential to make the connections short to minimize the resistance in the conductors. The best wiring connection that we came up with is seen in Figure 33.

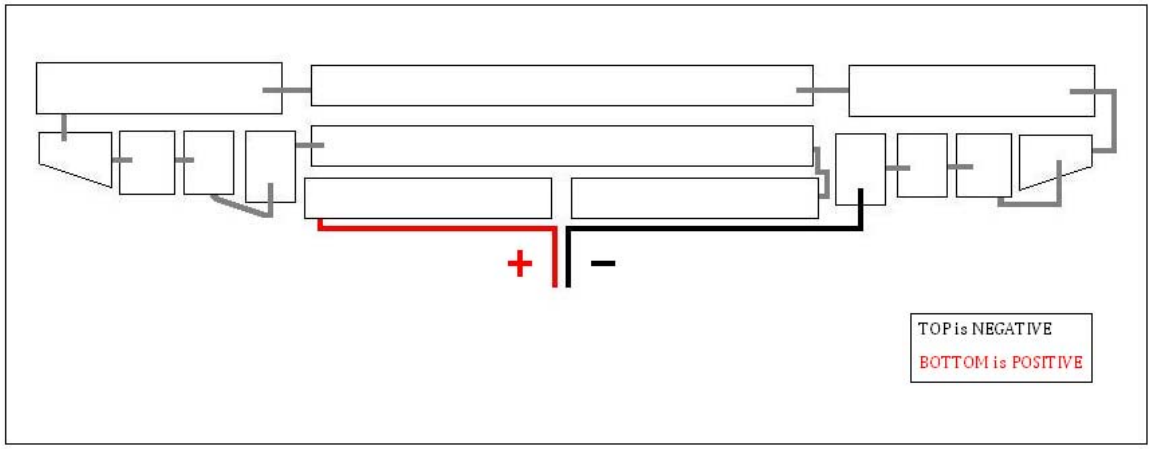

Figure 33. Solar Panel Wiring.

The final product is seen in Figure 34. The solar cells were attached to the wing with double sided tape. As mentioned earlier a second layer of carpet protection film was used to secure the solar cell arrangement on the wing.

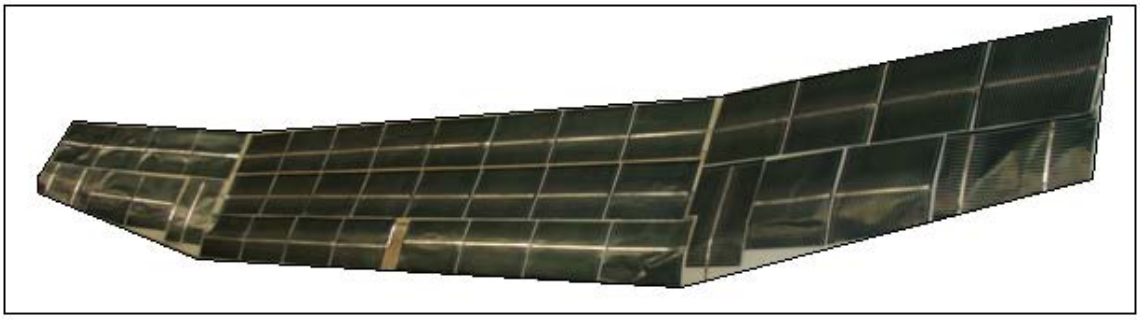

Figure 34. Solar Panel.

F. MAXIMUM POWER POINT TRACKER

As described in Chapters III and IV, different factors influenced the output of a solar cell, such as irradiance, temperature, angle of incidence, etc. Hence, the output power from the solar panel will always be fluctuating throughout the day. In order to get the most power from the panel, it was necessary to add into our circuitry a MPPT.

Additionally, we knew that the output voltage of the solar panel would be lower than the voltage required to charge the battery. Therefore, we needed a DC-DC power converter to continuously boost the voltage to 25.2V which was the voltage of the Li-ion battery.

While looking through the products and their respective manufacturers used in previous research [5], we came across a GVB24-6 Boost Solar Charge Controller from GENASUN Advanced Energy Systems, seen in Figure 35, which included both needed components, MPPT and boost converter. Since

the voltage of a Raven's fully charged battery was 25.2V, we asked the manufacturer to program the boost solar charge controller to that voltage value. In Table 5, the original specifications of the component are displayed.

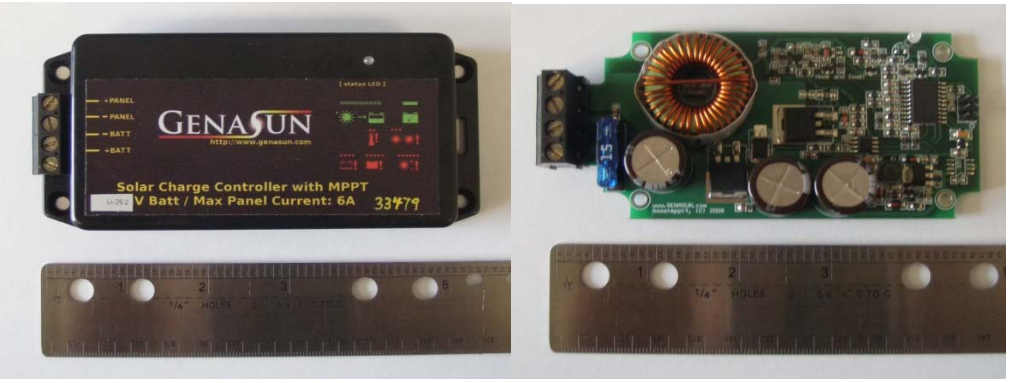

Figure 35. GV26-4 Boost Solar Charge Controller.

Table 5. GV24-6 Boost Specifications (After [41]).

Tracking Efficiency	99%
Electrical Efficiency (typical)	90-96%
Input Current (Maximum)	6A
Panel Voltage (Voc)	0-63V
Min. Panel Voltage for Charging	5V
Night Consumption	6mA
Absorption Voltage	28.4V
Float Voltage	27.6V
Temperature Compensation	56mV/°C
Compact and Light	5.5x2.5x1.2" (14x6.5x3.1 cm) / 6.5 oz. (185 g)
Connections	4-pos. clamp-style terminal block for 10-30AWG wire
Environmental	Stainless Hardware Nickel-Plated Brass Contacts
Additional Features	Multi-Stage Charging Temperature Compensation Can Charge from a DC Source Automatic Recovery from Fault Conditions LED Status Indicator Reverse Panel Protection Overload Protected (No blown fuses!) Over-Temperature Protected with Current Foldback Shade-Tolerant Tracking Suitable for Gel/AGM/Sealed Lead-Acid Batteries Surface-Mountable Box Reverse Battery Protection Custom Voltages Available for Lithium and Other Batteries

One concern we had when looking for electronic components was their weight and size. The MPPT/power converter (Solar Charge Controller) weighed 6.5-Oz, but without the casing it weighed only 3.6-Oz. We preferred to use it without the casing. The dimensions of the charge controller were 14cmx6.5cmx3.1cm. Besides the wing and the horizontal stabilizer, the Raven RQ-11B did not provide any other flat surface where additional components could be mounted. Internal compartments of the aircraft were taken with other payload components. The only area available was on top of

the fuselage, as seen in Figure 36. This location was ideal because it had enough space for the charge controller and the balancer charger and because it was close to the solar panel and to the battery, which reduced the amount of wiring needed for connections.

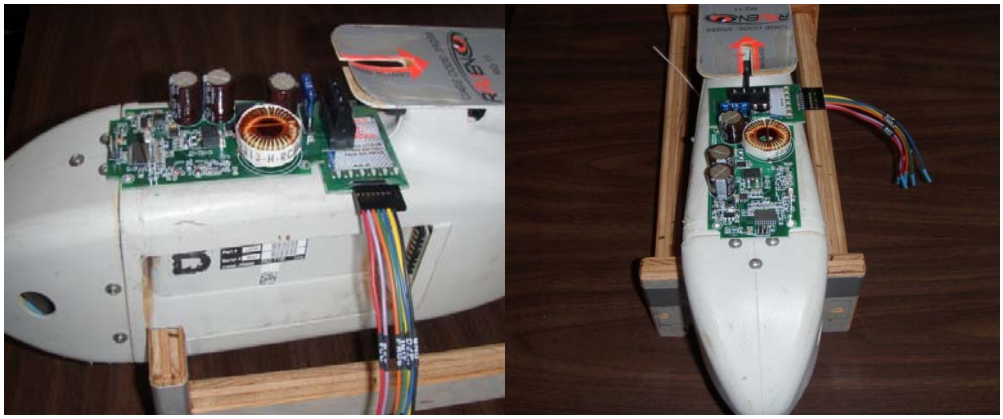

Figure 36. Integrated Circuit on Fuselage of Raven RQ-11B.

G. BALANCER CHARGER

As mentioned in Chapter IV, Li-ion batteries required extreme caution when charging. Since our objective was to recharge the battery during flight, it was important to ensure that the charge for each battery cell inside the battery pack was correctly balanced. To do that, we were required to use a balancer charger. There were many products available to choose from, but we decided to purchase the Ultra-Balancer from Common Sense RC. This balancer charger was designed to charge 2-6 Lithium Polymer battery packs. This balancer was ideal for this project because it was small in size and light-weight. Its dimensions were 4.1cm X 6.2cm and weighed 0.5-Oz. Another positive factor that helped gain confidence about this product was the fact it had been previously experimented with by engineers from Na-

val Air Warfare Station in China Lake, California. They obtained positive results and recommended this product. The balancer charger is shown in Figure 37.

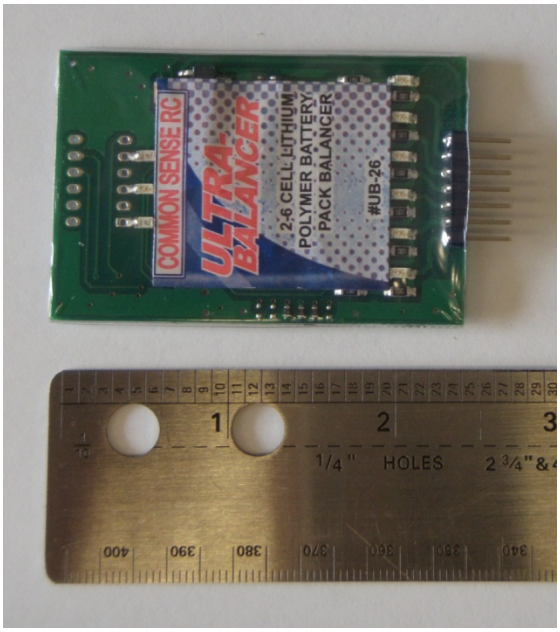

Figure 37. Ultra-Balancer Charger.

Another benefit of the balancer charger is that it contains three different color LED lights that makes the user aware of whether the voltage of one of the cells is below 3.2V, above 3.7V, or if they are equally charged, when conducting stationary tests. It has also six additional LED lights for every cell in the battery that alerts the user of any cell that higher voltage.

H. SYSTEM INTEGRATION

The final step in the design was the assembly and integration of all the components. The final circuitry design is shown in Figure 38. In the diagram below, the solar panel is connected to the MPPT. A diode P/N: HEP170 from Motorola was placed on the positive terminal of the

solar panel to prevent the battery from charging the solar panel, and thus, damaging the solar cells. The MPPT and the balancer charger were connected to the battery while the battery was powering the Raven UAV.

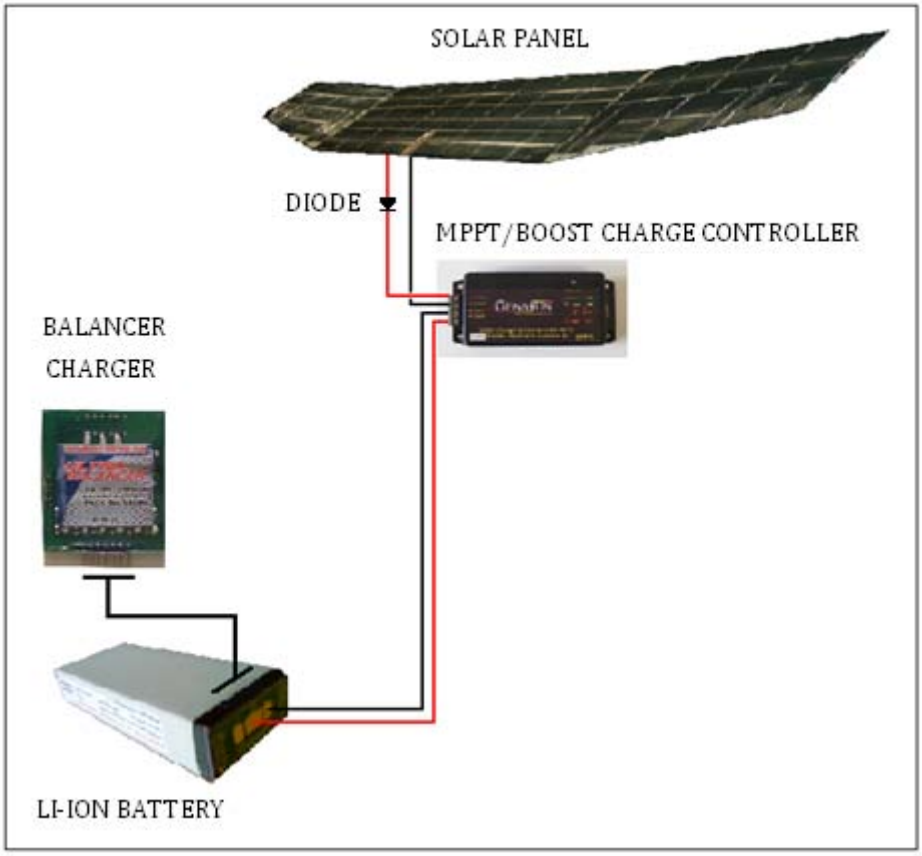

Figure 38. System Configuration.

Once the solar panel was constructed and all the other components were put in place, it was time to determine the amount of input power we would be getting from the sun and determine to whether it would actually extend the endurance of the battery. The next chapter shows the tests and results obtained from this circuit.

THIS PAGE INTENTIONALLY LEFT BLANK

VI. TEST AND ANALYSIS

A. LABVIEW

To facilitate our data collection, we needed some type of software that would enable us to take voltage and current readings simultaneously and autonomously between the solar panel (SP) and the MPPT, and between the battery and the Raven. For this purpose, we opted to use LABVIEW. From Figure 39, it can be seen how we connected our test equipment.

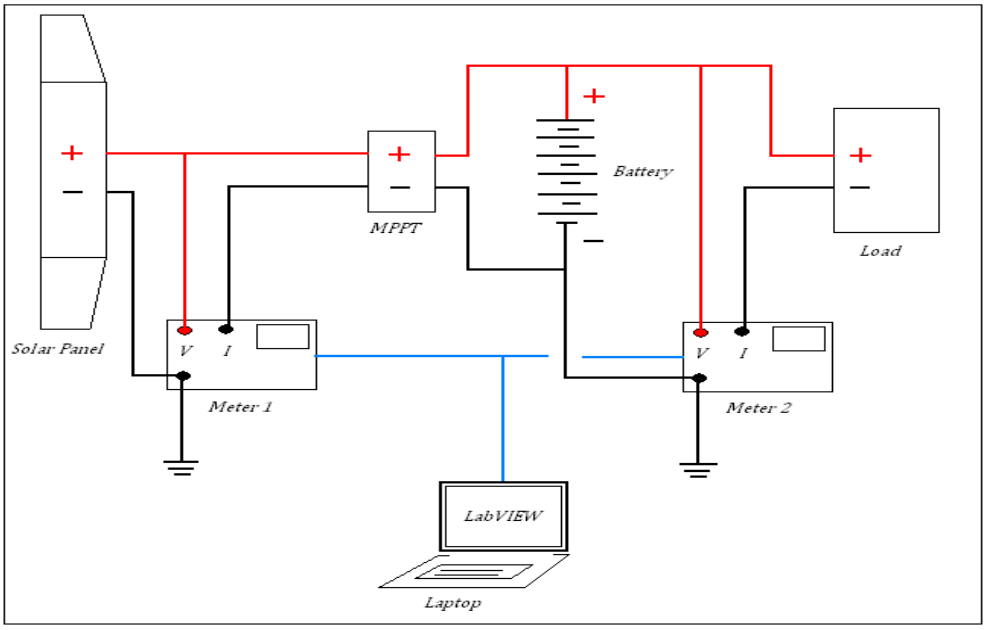

Figure 39. Test Equipment Connection.

LABVIEW is a graphical system design platform that allows engineers and scientists to interface with any measurement device and design tool. It is a programming language that has common programming devices like data types (numbers, strings, arrays, etc.), structures (For Loops, While Loops, case structures, event handling) and functions

(file I/O, comparisons, etc.) [42]. Nevertheless, it does not require any programming experience since it has built-in functions for common tasks such as data acquisition and analysis, and a wide array of tool kits and modules that offer specific functionality in areas such as real-time control, RF design, motion control and machine vision, etc.

For our experiment, we used two FLUKE multi-meters to interface with LABVIEW. Each one of these measurement devices had the option of taking two readings, simultaneously. We placed one multi-meter between the solar panel and the MPPT, and the other between the battery and the Raven UAV. We programmed LABVIEW so that it would take the two readings from each multi-meter every one second with use of a time stamp function. Additionally, we created an alarm function that would signal if the acquired battery voltage reading went below 21.2V. Finally, we added a chart that would enable to see how much power would be consumed by the battery, and how much power would be coming in from the solar panel.

The front panel of our program in LABVIEW is shown in Figure 40. The front panel displays controls and indicators. For our test, we used two separate LABVIEW front panels and block diagrams. The block diagram which is where the program was created is shown in Figure 41.

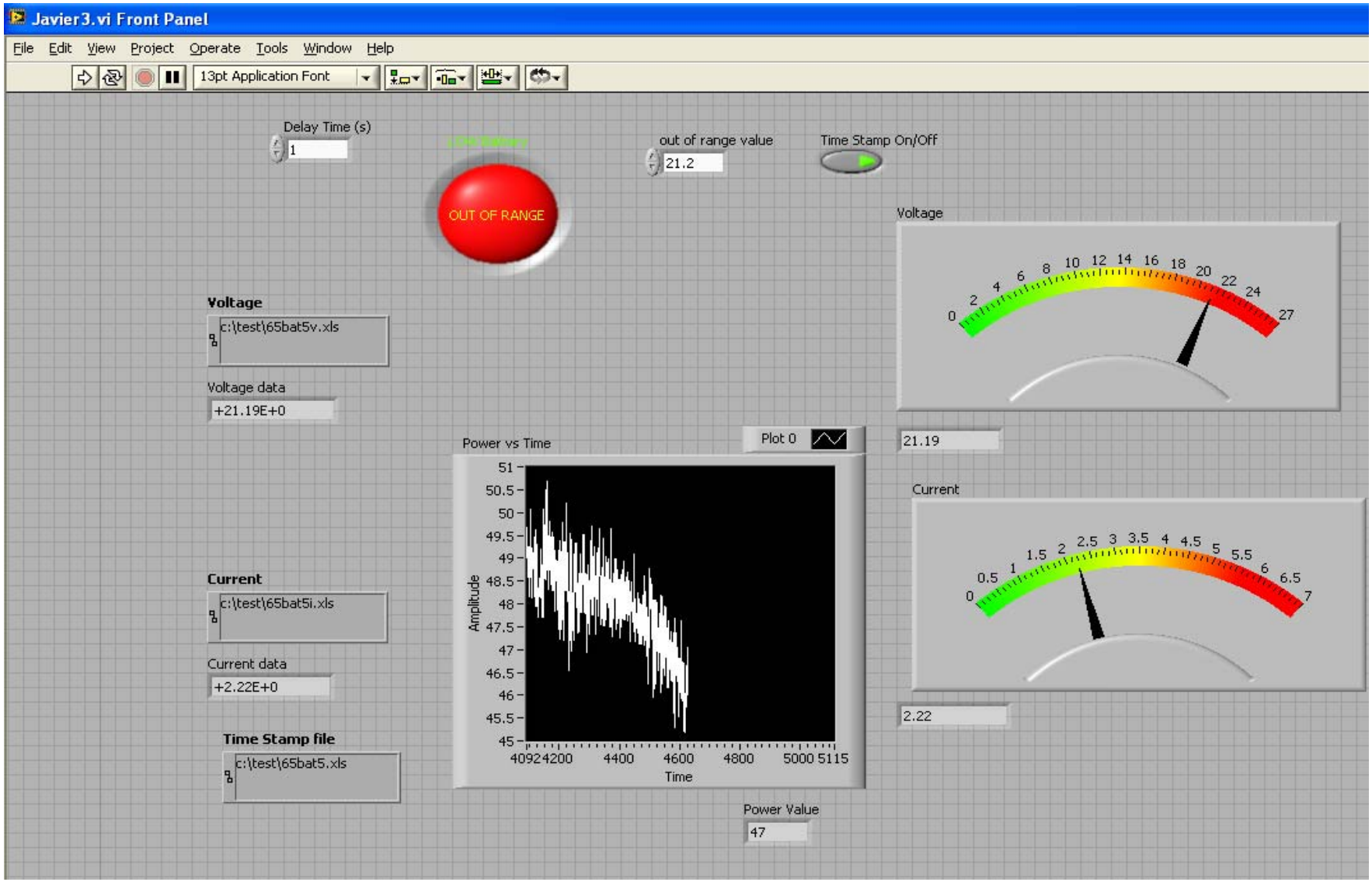

Figure 40. LABVIEW Front Panel.

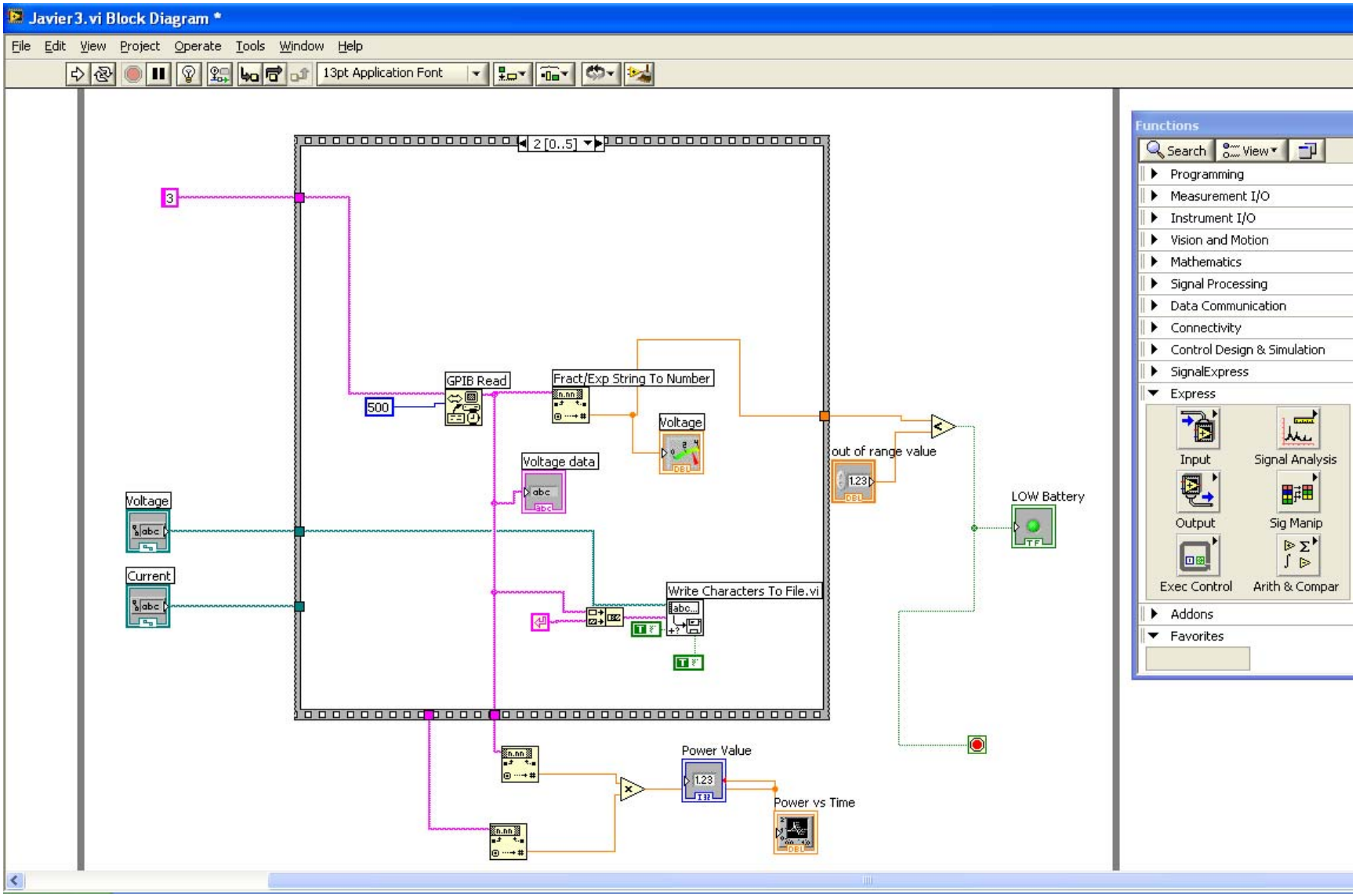

Figure 41. LABVIEW Block Diagram.

B. REFERENCE SOLAR CELL

A silicon solar cell was used to measure the intensity of the sunlight at every test to ensure that the tests were done under similar conditions. The silicon cell was connected to a multi-meter set to measure current and it was placed next to the solar panel and with the same angle facing the sun. Our tests were normally conducted between 11:00AM and 3:00PM and the readings were always between 0.27A and 0.31A. The highest current readings observed were in Carmel Valley, California. There, the current from the silicon cell stayed between 0.30A and 0.31A. The reference solar cell is shown in Figure 42.

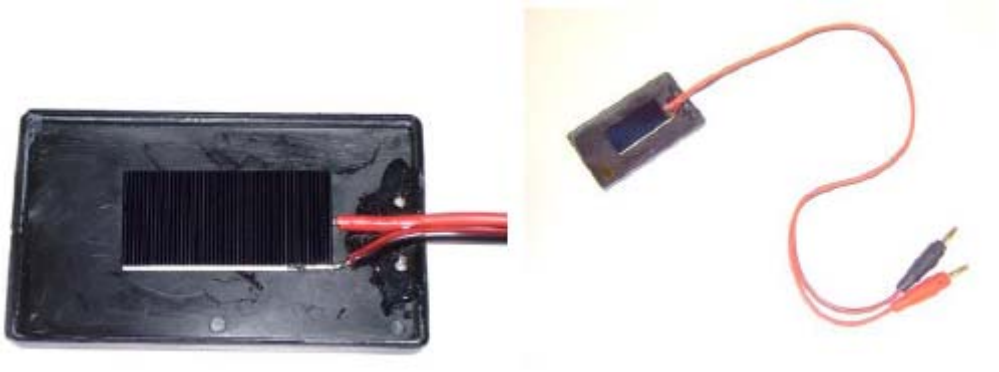

Figure 42. Reference Solar Cell (From [5]).

C. BATTERY CAPACITY TESTS

The Raven RQ-11B comes with six Li-ion polymer cells inside a battery pack. It has a fully charged voltage of 25.2V and a minimum voltage of 21V. It has a capacity of 4 Ampere hours (Ah) [17].

To better understand its capacity, we ran different tests while the battery was connected to the Raven at different throttle settings, which represented the actual op-

erating speeds of the UAV during regular missions. These settings were chosen by the Raven's operator, Mr. Scott Brown, a technician from the Naval Air Warfare Center Weapons Division, in China Lake, California [43].

We first obtained battery capacity and discharge rate values at 55%, 65%, 70%, and 100% throttle levels. Table 6 shows these results. We did several tests at each individual level and averaged them to ensure that our values were accurate. Table 6 also displays the capacity of the battery at different throttle levels.

Table 6. Raven Battery Capacity Bench Test.

Throttle	55%	65%	70%	100%
Avg. Current (A)	1.32	1.64	1.75	5.43
Avg. Voltage (V)	22.7	22.96	22.4	21.72
Time (hours)	1	1	1	1
Avg. Resistance	17.19	14	12.80	4
Capacity (Ah)	1.32	1.64	1.75	5.43

The capacity C of the battery was calculated by multiplying the average current I_{avg} by the time t it took for the battery to reach 21.2V, as seen in equation 6.1 [44].

$$C = I_{avg} * t \tag{5.5}$$

For our cut-off low voltage, we used a conservative battery voltage value of 21.2V to ensure the battery would not over-discharge; thus, running the risk of damaging the battery, as it was explained in the previous chapter.

D. ENERGY CALCULATIONS

According to the Raven's operator, during launching and up to the point where the SUAV reaches altitude, the Raven is operated at 100% throttle. This stage takes about 10 minutes. Once a specific altitude is reached, the operator reduces its speed controlling the throttle between 55% and 65% for the remaining of the mission. With this in mind, it was time to calculate the amount of energy the battery would use during the initial 10 minutes at 100% and the energy used for the rest of the time at 55%, 65%, and 70%. Our initial calculations were determined at 55% throttle, initially. Our goal was to determine the amount of time the Raven would fly under those throttle conditions.

1. Fully Charged Battery

We began by calculating the energy of a fully charged battery, given the capacity of 4Ah, by multiplying the voltage of the battery times its capacity.

$$E = V * C \tag{5.6}$$

In equation 6.2, E represents energy in Watt hours (Wh), V is the voltage of the battery in Volts, and C is its capacity in Ampere hours. We did not intend to use all of its capacity because the minimum voltage was 21V. However, we decided to use a more conservative value 21.2V to ensure we do not go below the minimum required voltage set by the manufacturer. Hence, we used 85% of its capacity which gave us 3.4Ah. Additionally, we used the minimum allowable battery voltage reading of 23.9V, which was the fully charged voltage reading when the battery was connected to the load, instead of the 25.2V given by the manufacturer.

We did this because wanted to get a value that would represent the actual condition of the battery as it prepares to launch. The maximum and actual minimum energy results are shown in Table 7.

Table 7. Energy of a Fully Charged Battery.

	Voltage (V)	Capacity (Ah)	Energy (Wh)	Energy (J)
Maximum	25.2	4	100.8	363K
Actual (min)	21.2	3.4	72.08	260K

2. Raven's Energy Consumption

Next, we calculated the energy that the Raven would use in a single mission at full throttle (100%) for the first 10 minutes. Using equation (6.2) and the values obtained in Tables 6 and 7, we calculated the energy to be:

$$E = (23.9V)(5.43Ah)(0.1667h) = 21.63Wh \qquad (5.7)$$

In our previous tests, we noticed that after running the Raven for 10 minutes at full throttle the battery voltage usually dropped about 1V. Thus, we used this fact to calculate the energy at 55% power.

$$E = (22.9V)(1.32Ah)(1h) = 30.23Wh \qquad (5.8)$$

Notice that after 1 hour and 10 minutes the total energy used was calculated to be 51.86Wh. The energy values calculated at these throttle levels can be seen in Table 8.

Table 8. Energy and Time Used at 100% and 55% throttle.

	100%	55%	Subtotal	Extra Time	Total
Energy (Wh)	21.63	30.23	51.86		
Time	10min	1h	1h 10min	40min	1h 50min

Since the energy of a fully charged battery was 72.08 Wh (Table 7), there was 20.22Wh of energy left which indicated that the Raven would run for another 40 minutes at

55% throttle. Hence, the battery would have a total time of duration of 1 hour and 50 minutes before it discharges down to 21.2V under 100% and then 55% throttle settings.

Similarly, as seen in Tables 9 and 10, we calculated the amount of time the battery would take to discharge from 100% to 65% and from 100% to 70% throttle levels.

Table 9. Energy Used at 100% and 65% throttle.

	100%	65%	Subtotal	Extra Time	Total
Energy (Wh)	21.63	37.56	59.19		
Time	10min	1h	1h 10min	21min	1h 31min

Table 10. Energy Used at 100% and 70% throttle.

	100%	70%	Subtotal	Extra Time	Total
Energy (Wh)	21.63	40.08	61.70		
Time	10min	1h	1h 10min	16min	1h 26min

3. Load Energy Consumption

Before we integrated our solar panel into the Raven's circuitry, we wanted to implement our calculation with a load similar to the Raven's payload to ensure that our method would work. For this, we obtained two high wattage resistors of 3.8-Ohms and 9.5-Ohms. We used the 3.8-Ohms resistor to simulate the Raven UAV operating at 100% throttle, and the 9.5-Ohms resistor to simulate operation at 55%, respectively. Figure 43 shows the high power resistors used to represent the Raven's payload. The 3.8-Ohms resistor is at the top, and the 9.5-Ohm resistor is shown at the bottom.

Figure 43. High Power Resistors.

Since our resistances were not exactly the same as those obtained in Table 6, we had to calculate a new capacity value $C_{Battery\,w/\,Load}$ using the ratio of resistances, as seen in equation 6.5, where R_{Raven} represented the resistance of the Raven, $R_{High-wattage}$ was the resistance of the high power resistor, and $C_{Battery\,w/\,Raven}$ represented the capacity obtained previously.

$$C_{Battery\,w/\,Load} = \frac{R_{Raven}}{R_{high-wattage}} * C_{Battery\,w/\,Raven} \tag{5.9}$$

From Table 11, it can be seen the new battery capacity values for the corresponding similar loads.

Table 11. Battery Capacity Similar Load.

Throttle	R Raven	R Load	C w/ Raven	C w/ Load
100%	4Ω	3.8Ω	5.43 Ah	5.71 Ah
55%	17.25Ω	13.3Ω	1.32 Ah	1.71 Ah

With these capacity values, we calculated the energy used by battery under these comparable loads using equations 6.3 and 6.4. The energy used by the battery under a similar load to the Raven's is shown in Table 12.

Table 12. Energy Used and Battery Endurance w/ Similar Load.

Throttle Level	100%	55%		55%
Elapsed Time (min)	+10	+60		+16
Energy Fully Charged Battery			72.08	
Energy Out - Load (Wh)	22.79	39.15	61.94	10.14
Energy In – Solar Panel (Wh)				10.14
Energy Left after 1hr 10 min (Wh)			10.14	
Energy Left after extra 16 min (Wh)				0.00
Total Elapsed Time 86 min = 1 hr 26 min				

Since the energy of a fully charged battery was 72.08Wh (Table 7), there were 10.14Wh of energy left, which indicated that the Raven would run for another 16 minutes. Therefore, the battery would have a total time of duration of 1 hour and 26 minutes before it discharges down to 21.2V at 100% and 55% throttle settings.

E. BATTERY ENDURANCE TESTS

1. Raven's Energy Consumption

To ensure our calculations taken in the previous section were correct, we tested the battery while connected to the Raven and let it run under those settings (100-55% throttle). A comparison between our calculated time, from section C-2, and the actual time is shown in Table 13.

Table 13. Calculated vs. Actual Time (100-55%).

	Time
Calculated	1h 50min
Actual Test	1h 53min

As expected, a small difference was observed mostly due to the different voltage levels among fully charged batteries. As seen in Figure 44, the battery power consumption at 100% to 55% throttle lasted 6,780-seconds.

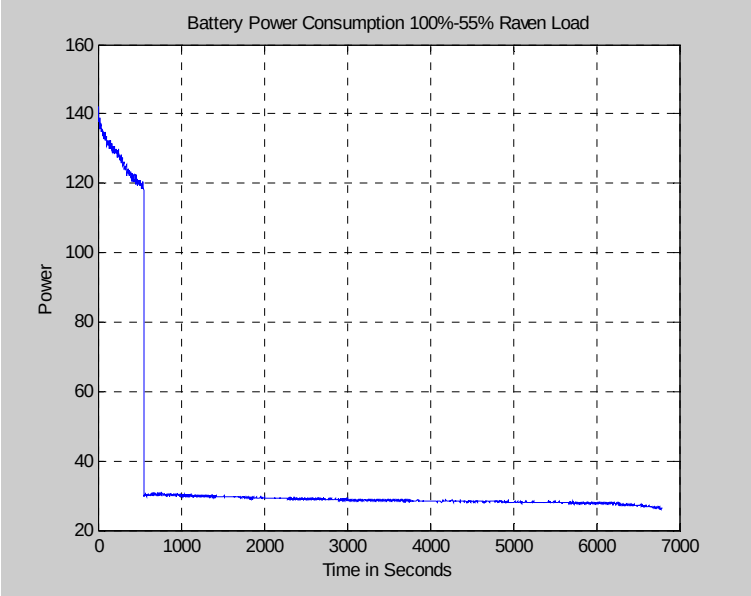

Figure 44. Power Consumption 100% to 55% Raven.

In similar fashion, we tested the power consumption of the battery while connected to the Raven at 100% and 65% and at 100% and 70% throttle levels. The relationship between the calculated times and the actual times obtained from the test is observed in Tables 14 and 15.

Table 14. Calculated vs. Actual Time (100-65%).

	Time
Calculated	1h 31min
Actual Test	1h 34min

Table 15. Calculated vs. Actual Time (100-70%).

	Time
Calculated	1h 26min
Actual Test	1h 26min

Again, we observed a small difference between our calculated values and our actual test, but for the most part it indicated that our calculations were correct. The power consumption of the battery under those specific throttle settings are seen in Figures 45 and 46, respectively. In Figure 45, we noticed how the battery of the Raven lasted 5,640-seconds, while operating at 100% and then at 65% throttle.

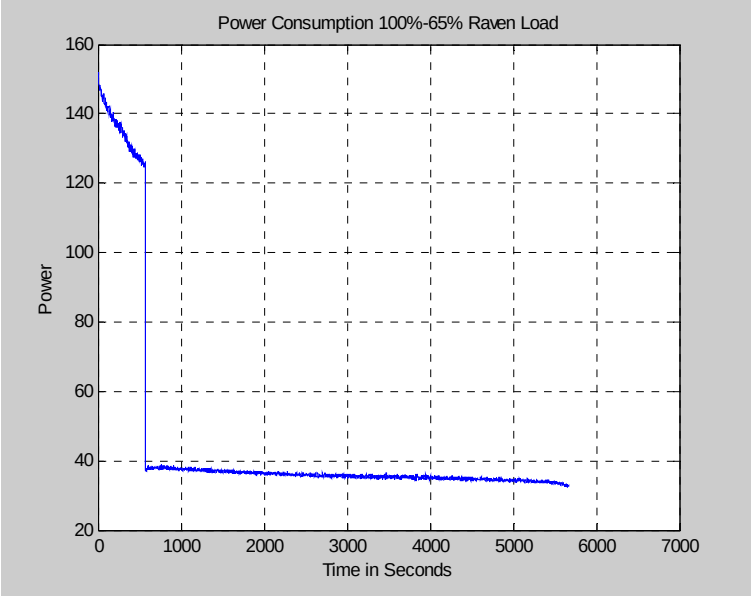

Figure 45. Power Consumption 100% to 65% Raven.

In Figure 46, we observed that the battery of the Raven UAV lasted 5,160-seconds, while operating at 100% and then at 70% throttle settings.

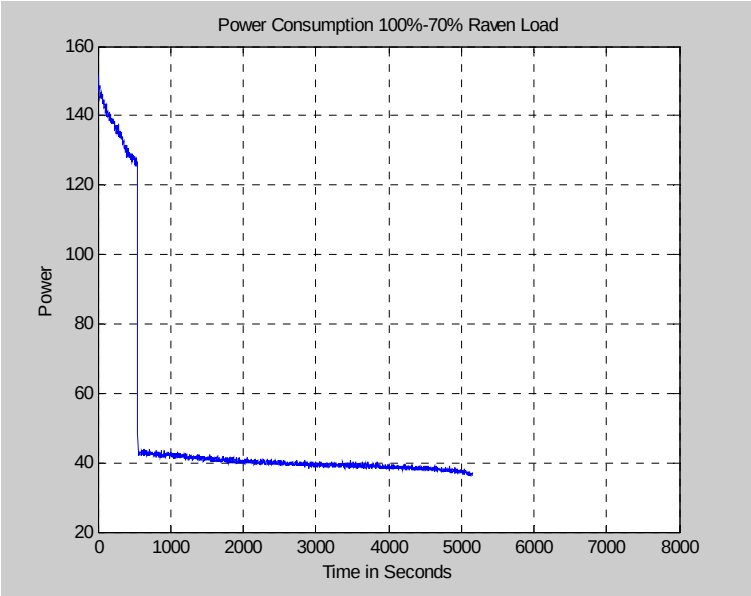

Figure 46. Power Consumption 100% to 70% Raven.

2. Load Energy Consumption

Again, to ensure our calculations from section C-3 were correct, we tested the battery while connected to the load similar to the Raven's. A comparison between our calculated time and the actual time is observed in Table 16.

Table 16. Calculated vs. Actual Time Similar Load.

	Time
Calculated	1h 26min
Actual Test	1h 29min

The results in Table 16 show that our computations were correct. In Figure 47, we observe the power consumption of the battery while connected to a similar load. Again, this test represented the Raven RQ-11B load operating at 100% throttle for the first 10 minutes and at 55% throttle for the rest of the time. In Figure 47, it can be seen that the power of the battery lasted 5,340-seconds under a similar load

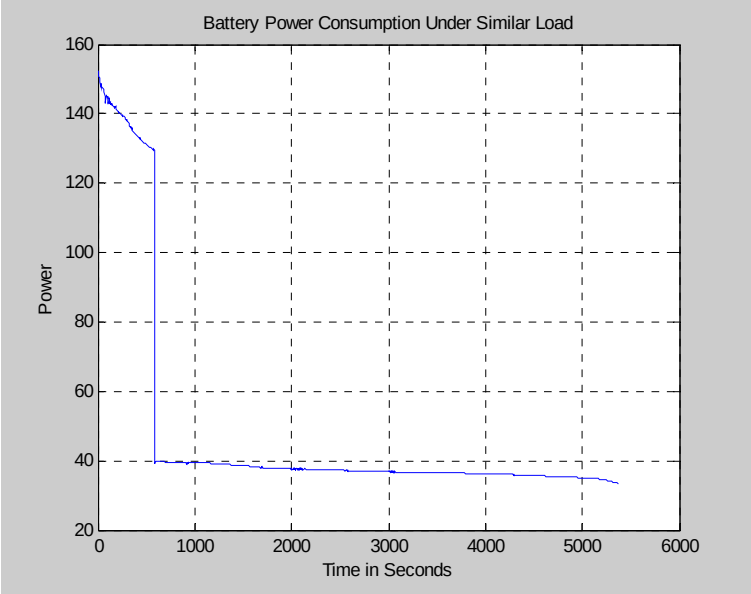

Figure 47. Power Consumption 100% to 55% Similar Load.

F. BATTERY ENDURANCE CALCULATIONS WITH SOLAR PANEL

1. Load with Solar Panel

After confirming that our calculations matched our test results, we wanted to add the input from the solar panel into our calculations. Previously, we conducted several tests to determine the IV curve of the solar panel that we built. The IV curve obtained from our solar panel on 3 August 2010 is shown in Figure 48.

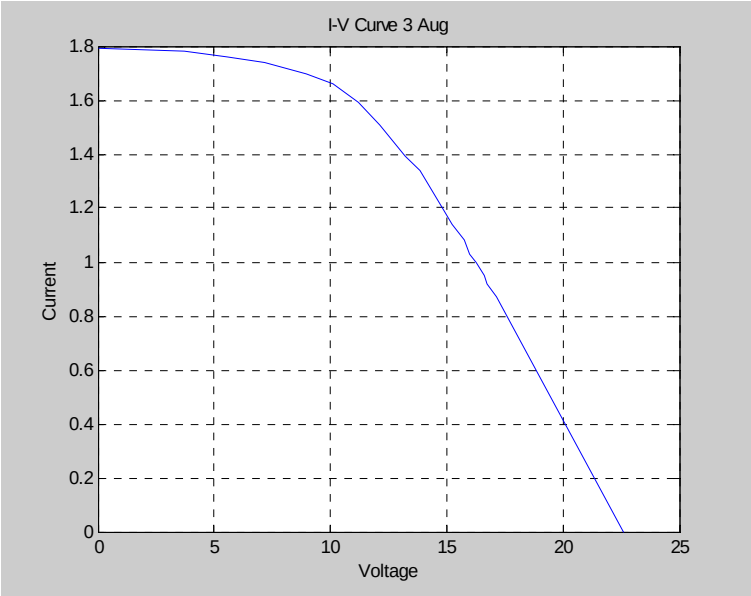

Figure 48. IV Curve Plot for Wing Solar Panel.

In Figure 48, we noticed that the knee of curve indicated that the maximum power was somewhere around 17W. In addition, we noted that throughout most part the day, the solar panel would provide 12W of power to the battery. Therefore, we used 17Wh and 12Wh in our calculations as our energy input boundaries to represent our best and worst case energy input in relation to the Monterey Area. The

amount of time the battery would last while connected to a similar load would depend on the amount of energy left in it.

Following the same calculations as in the previous sections, we obtained the amount of time it would take for the battery to discharge to 21.2V, as seen in Table 17.

Table 17. Battery Endurance Calculation Load w/SP (17Wh).

Throttle Level	100%	55%		55%	55%	55%	55%
Elapsed Time (min)	10	60		45	19	8	3
Energy Fully Charged Battery			72.08				
Energy Out - Load (Wh)	22.77	39.16	61.93	29.60	12.59	5.36	2.28
Energy In – Solar Panel (Wh)	2.84	17.00	19.84	12.85	5.47	2.33	0.99
MPPT 2% Power Loss	0.06	0.34	0.40	0.26	0.11	0.05	0.02
Energy Gain (Wh)			29.60				
Energy Gain (Wh)				12.59			
Energy Gain (Wh)					5.36		
Energy Gain (Wh)						2.28	
Energy Gain (Wh)							0.97
Average Energy Input (Wh)	17.00	17.00		17.00	17.00	17.00	17.00
Total Elapsed Time (min)	146						
Total Elapsed Time (hr)(min)	2	26					

Since the total energy of the battery (Table 7) was 72.08Wh, it meant that the battery would have 29.60Wh of energy left. This would give us an additional 45 minutes to the time obtained in Table 12, i.e., only if the solar panel would stop providing energy. Nevertheless, we expected the solar panel to be connected to the battery during those extra 45 minutes; hence, overall we would get additional 30 minutes of energy at 17Wh of constant input. As a result, our calculations predicted 60 minutes of extra time, which total 2 hours and 26 minutes compared to the 1

hour and 26 minutes given by the battery alone (Table 12). Overall, we estimated a 70% improvement in battery endurance.

Following the same calculation method seen in Table 17, we noticed that for an average energy input of 12Wh, we would get a total of 36 minutes of extra time, giving a total of 122 minutes or 2 hours and 2 minutes of battery endurance. In this case, we observed a 42% improvement in battery endurance. These calculations are shown in Table 18.

Table 18. Battery Endurance Calculation Load w/SP (12Wh).

Throttle Level	100%	55%		55%	55%	55%	55%
Elapsed Time (min)	10	60		37	11	3	1
Energy Fully Charged Battery			72.08				
Energy Out - Load (Wh)	22.77	39.16	61.93	23.88	7.17	2.15	0.65
Energy In – Solar Panel (Wh)	2.00	12.00	14.00	7.32	2.20	0.66	0.20
MPPT 2% Power Loss	0.04	0.24	0.28	0.15	0.04	0.01	0.00
Energy Gain (Wh)			23.88				
Energy Gain (Wh)				7.17			
Energy Gain (Wh)					2.15		
Energy Gain (Wh)						0.65	
Energy Gain (Wh)							0.19
Average Energy Input (Wh)	12.00	12.00		12.00	12.00	12.00	12.00
Total Elapsed Time (min)	122						
Total Elapsed Time (hr)(min)	2	2					

In Table 19, we can appreciate the difference in battery endurance between our calculations with and without solar panel at certain energy input levels. As explained before, we used 12Wh and 17Wh as our low and maximum input energy levels.

Table 19. Battery Endurance w/Load.

Calculations	Energy IN from SP	Time	Improvement
Load w/o SP	0Wh	1h 26min	0%
Load w/ SP	12Wh	2h 2min	42%
Load w/ SP	17Wh	2h 26min	70%

2. Raven with Solar Panel (100%-55%)

Similarly, it was necessary to calculate the energy going into the battery and the energy coming out of the battery to determine the amount of time the battery would last.

From Table 8, we knew that the energy used by the Raven at 100% for the first 10 minutes was 21.63Wh and 30.23Wh at 55% for 1 hour; hence, we estimated the time the battery would last, as seen in Tables 20 and 21. To better estimate the time, we made our calculations using a low energy average input value of 12Wh, to represent worst irradiance conditions, and 17Wh, to represent sunny conditions. In Table 20, we observe the results obtained for an average input energy of 12Wh. From Table 21, it can be seen the results obtained for an average input of 17Wh.

Table 20. Battery Endurance Calculation Raven w/SP (100%-55% Throttle) 12Wh Energy Input.

Throttle Level	100%	55%		55%	55%	55%	55%	55%	55%
Elapsed Time (min)	10	60		67	26	10	4	2	1
Energy Fully Charged Battery			72.08						
Energy Out - Raven (Wh)	21.63	30.23	51.86	33.95	13.21	5.14	2.00	0.78	0.30
Energy In – Solar Panel (Wh)	2.00	12.00	14.00	13.48	5.24	2.04	0.79	0.31	0.12
MPPT 2% Power Loss	0.04	0.24	0.28	0.27	0.10	0.04	0.02	0.01	0.00
Energy Gain (Wh)			33.95						
Energy Gain (Wh)				13.21					
Energy Gain (Wh)					5.14				
Energy Gain (Wh)						2.00			
Energy Gain (Wh)							0.78		
Energy Gain (Wh)								0.30	
Energy Gain (Wh)									0.12
Average Energy Input (Wh)	12.00	12.00		12.00	12.00	12.00	12.00	12.00	12.00
Total Elapsed Time (min)	180								
Total Elapsed Time (hr)(min)	3	0							

Table 21. Battery Endurance Calculation Raven w/SP (100%-55% Throttle) 17Wh Energy Input.

Throttle Level	100%	55%		55%	55%	55%	55%	55%	55%	55%
Elapsed Time (min)	10	60		79	43	24	13	7	4	2
Energy Fully Charged Battery			72.08							
Energy Out - Raven (Wh)	21.63	30.23	51.86	39.66	21.86	12.05	6.64	3.66	2.02	1.11
Energy In – Solar Panel (Wh)	2.84	17.00	19.84	22.31	12.29	6.78	3.73	2.06	1.13	0.63
MPPT 2% Power Loss	0.06	0.34	0.40	0.45	0.25	0.14	0.07	0.04	0.02	0.01
Energy Gain (Wh)			39.66							
Energy Gain (Wh)				21.86						
Energy Gain (Wh)					12.05					
Energy Gain (Wh)						6.64				
Energy Gain (Wh)							3.66			
Energy Gain (Wh)								2.02		
Energy Gain (Wh)									1.11	
Energy Gain (Wh)										0.61
Average Energy Input (Wh)	17.00	17.00		17.00	17.00	17.00	17.00	17.00	17.00	17.00
Total Elapsed Time (min)	243									
Total Elapsed Time (hr)(min)	4	3								

As seen in Table 22, our calculations predicted that, under those specific average energy input conditions, the Raven UAV with solar panel can last 64% and 121% longer, compared to the almost two hours that it will endure without a solar panel.

Table 22. Battery Endurance Raven w/SP (100%-55%).

Calculations	Energy IN from SP	Time	Improvement
Raven w/o SP	0Wh	1h 50min	0%
Raven w/ SP	12Wh	3h	64%
Raven w/ SP	17Wh	4h 3min	121%

3. Raven with Solar Panel (100%-65%)

After obtaining the calculations for the Raven while operating at 100% and 55% throttle levels with a solar panel attached, it was necessary to do the same thing but for the next set of throttle settings (100%-65%), described by the Raven's operator. The energy used and battery endurance under a constant energy input of 12Wh and 17Wh are shown in Tables 23 and 24, respectively.

Table 23. Battery Endurance Calculation Raven w/SP (100%-65% Throttle) 12Wh Energy Input.

Throttle Level	100%	65%		65%	65%	65%	65%
Elapsed Time (min)	10	60		43	13	4	1
Energy Fully Charged Battery			72.08				
Energy Out - Raven (Wh)	21.63	37.56	59.19	26.62	8.34	2.61	0.82
Energy In – Solar Panel (Wh)	2.00	12.00	14.00	8.51	2.66	0.83	0.26
MPPT 2% Power Loss	0.04	0.24	0.28	0.17	0.05	0.02	0.01
Energy Gain (Wh)			26.62				
Energy Gain (Wh)				8.34			
Energy Gain (Wh)					2.61		
Energy Gain (Wh)						0.82	
Energy Gain (Wh)							0.26
Average Energy Input (Wh)	12.00	12.00		12.00	12.00	12.00	12.00
Total Elapsed Time (min)	132						
Total Elapsed Time (hr)(min)	2	12					

Table 24. Battery Endurance Calculation Raven w/SP (100%-65% Throttle) 17Wh Energy Input.

Throttle Level	100%	65%		65%	65%	65%	65%	65%	65%
Elapsed Time (min)	10	60		52	23	10	5	2	1
Energy Fully Charged Battery			72.08						
Energy Out - Raven (Wh)	21.63	37.56	59.19	32.34	14.34	6.36	2.82	1.25	0.56
Energy In – Solar Panel (Wh)	2.84	17.00	19.84	14.64	6.49	2.88	1.28	0.57	0.25
MPPT 2% Power Loss	0.06	0.34	0.40	0.29	0.13	0.06	0.03	0.01	0.01
Energy Gain (Wh)			32.34						
Energy Gain (Wh)				14.34					
Energy Gain (Wh)					6.36				
Energy Gain (Wh)						2.82			
Energy Gain (Wh)							1.25		
Energy Gain (Wh)								0.56	
Energy Gain (Wh)									0.25
Average Energy Input (Wh)	17.00	17.00		17.00	17.00	17.00	17.00	17.00	17.00
Total Elapsed Time (min)	163								
Total Elapsed Time (hr)(min)	2	43							

In Table 23, we observed a 45% improvement of the battery endurance thanks to the solar panel. The battery was expected to last 41 minutes longer, than without solar cells. In Table 24, the improvement was even higher due to the high input energy of 17Wh. All these observations are summarized in Table 25.

Table 25. Battery Endurance Raven w/SP (100%-65%).

Calculations	Energy IN from SP	Time	Improvement
Raven w/o SP	0Wh	1h 31min	0%
Raven w/ SP	12Wh	2h 12min	45%
Raven w/ SP	17Wh	2h 43min	79%

4. Raven with Solar Panel (100%-70%)

Finally, we did the same calculation with a higher throttle setting of 70% to cover all the speed control levels chosen by the operator. In Table 26, we expected the battery to last 36 minutes longer than without solar cells.

Table 26. Battery Endurance Calculation Raven w/SP (100%-70% Throttle) 12Wh Energy Input.

Throttle Level	100%	70%		70%	70%	70%	70%
Elapsed Time (min)	10	60		36	11	3	1
Energy Fully Charged Battery			72.08				
Energy Out - Raven (Wh)	21.63	40.08	61.70	24.10	7.07	2.08	0.61
Energy In – Solar Panel (Wh)	2.00	12.00	14.00	7.22	2.12	0.62	0.18
MPPT 2% Power Loss	0.04	0.24	0.28	0.14	0.04	0.01	0.00
Energy Gain (Wh)			24.10				
Energy Gain (Wh)				7.07			
Energy Gain (Wh)					2.08		
Energy Gain (Wh)						0.61	
Energy Gain (Wh)							0.18
Energy Gain (Wh)							
Energy Gain (Wh)							
Energy Gain (Wh)							
Average Energy Input (Wh)	12.00	12.00		12.00	12.00	12.00	12.00
Total Elapsed Time (min)	121						
Total Elapsed Time (hr)(min)	2	1					

Similarly, in Table 27 we expected a greater improvement since the energy input was higher. This time, the battery could last an extra hour, according to our calculations.

Table 27. Battery Endurance Calculation Raven w/SP (100%-70% Throttle) 17Wh Energy Input.

Throttle Level	100%	70%		70%	70%	70%	70%	70%	70%
Elapsed Time (min)	10	60		45	19	8	3	1	1
Energy Fully Charged Battery			72.08						
Energy Out - Raven (Wh)	21.63	40.08	61.70	29.82	12.40	5.15	2.14	0.89	0.37
Energy In – Solar Panel (Wh)	2.84	17.00	19.84	12.65	5.26	2.19	0.91	0.38	0.16
MPPT 2% Power Loss	0.06	0.34	0.40	0.25	0.11	0.04	0.02	0.01	0.00
Energy Gain (Wh)			29.82						
Energy Gain (Wh)				12.40					
Energy Gain (Wh)					5.15				
Energy Gain (Wh)						2.14			
Energy Gain (Wh)							0.89		
Energy Gain (Wh)								0.37	
Energy Gain (Wh)									0.15
Energy Gain (Wh)									
Average Energy Input (Wh)	17.00	17.00		17.00	17.00	17.00	17.00	17.00	17.00
Total Elapsed Time (min)	146								
Total Elapsed Time (hr)(min)	2	26							

In Table 28, we can compare the battery endurance calculated for the Raven with and without solar cells and its corresponding improvement.

Table 28. Battery Endurance Raven w/SP (100%-70%).

Calculations	Energy IN from SP	Time	Improvement
Raven w/o SP	0Wh	1h 25min	0%
Raven w/ SP	12Wh	2h 1min	42%
Raven w/ SP	17Wh	2h 26min	72%

G. BATTERY ENDURANCE TESTS WITH SOLAR PANEL

Our initial test was conducted in the Monterey Bay Area, but due to the variable weather conditions, we had to find a way to take the test equipment to a location where clear skies and good sunlight could be available throughout the day. As seen in Figure 49, we found a way to mount all the test equipment on a mid-size pick-up and travelled to Carmel Valley and Salinas in California, where the weather conditions were more accommodating for our research.

Figure 49. Mobile Laboratory.

1. Load with Solar Panel

To validate the calculations obtained in section E-1, it was necessary to test the solar panel while connected to the MPPT, battery, and to the load. We did two tests on

three separate days. Test 1 was interrupted due to heavy clouds and lack of sunlight; hence, it was completed in two days.

As seen in Figure 50, the input energy coming from the solar panel into the battery was different each test day. During the first test, we observed an initial average input energy of 16.45Wh. During the second part of the test, we noticed that the energy input increased and stayed fixed around 17.24Wh. Using the same method of calculation as in the previous sections, we decided to use the average of these two values (16.85Wh) as our energy input from our solar panel. Our estimated time of duration of 2 hours and 25 minutes is shown in Table 29.

Table 29. Battery Endurance Calculation Load w/SP Test 1.

Throttle Level	100%	55%		55%	55%	55%	55%
Elapsed Time (min)	10	60		45	19	8	3
Energy Fully Charged Battery			72.08				
Energy Out - Load (Wh)	22.77	39.16	61.93	29.42	12.41	5.23	2.21
Energy In – Solar Panel (Wh)	2.81	16.85	19.66	12.66	5.34	2.25	0.95
MPPT 2% Power Loss	0.06	0.34	0.39	0.25	0.11	0.05	0.02
Energy Gain (Wh)			29.42				
Energy Gain (Wh)				12.41			
Energy Gain (Wh)					5.23		
Energy Gain (Wh)						2.21	
Energy Gain (Wh)							0.93
Average Energy Input (Wh)	16.85	16.85		16.85	16.85	16.85	16.85
Total Elapsed Time (min)	145						
Total Elapsed Time (hr)(min)	2	25					

The second test had an average input energy of 14.55Wh. Similarly, we use this value to calculate our time of duration. The time duration of 2 hours and 13 minutes is reflected in Table 30.

Table 30. Battery Endurance Calculation Load W/SP Test 2.

Throttle Level	100%	55%		55%	55%	55%	55%
Elapsed Time (min)	10	60		41	15	5	2
Energy Fully Charged Battery			72.08				
Energy Out - Load (Wh)	22.77	39.16	61.93	26.79	9.76	3.55	1.29
Energy In – Solar Panel (Wh)	2.43	14.55	16.98	9.96	3.63	1.32	0.48
MPPT 2% Power Loss	0.05	0.29	0.34	0.20	0.07	0.03	0.01
Energy Gain (Wh)			26.79				
Energy Gain (Wh)				9.76			
Energy Gain (Wh)					3.55		
Energy Gain (Wh)						1.29	
Energy Gain (Wh)							0.47
Average Energy Input (Wh)	14.55	14.55		14.55	14.55	14.55	14.55
Total Elapsed Time (min)	133						
Total Elapsed Time (hr)(min)	2	13					

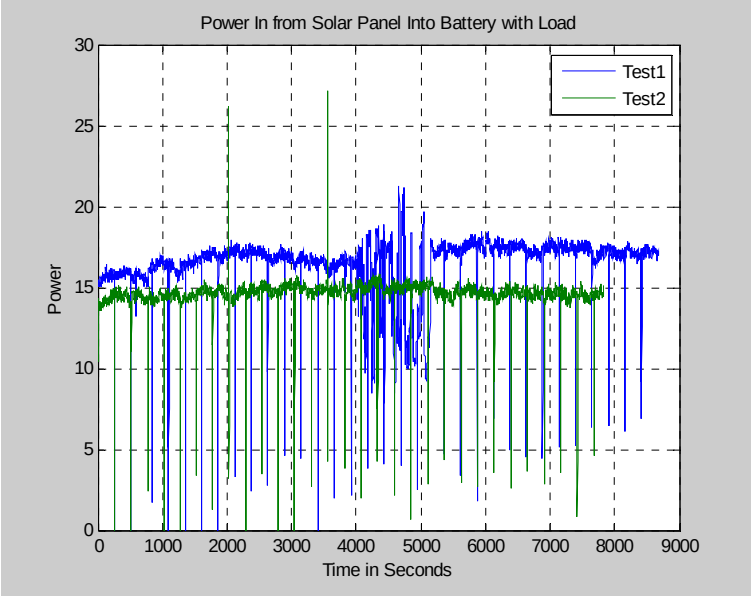

Figure 50. Power Input to Load w/SP Test.

In Figure 51, we decided to plot the power consumption of the battery without the solar panel, as seen in section D-2 to compare it with the actual test results obtained with the solar panel. During test 1, the power of the bat-

tery was consumed in 2 hours and 24 minutes. On test day 2 the battery lasted 2 hours and 10 minutes.

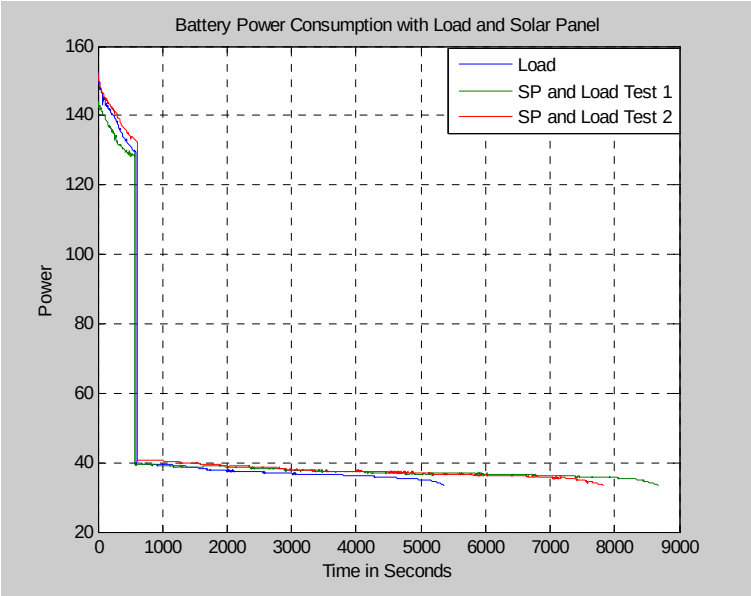

Figure 51. Power Consumption Load w/ Solar Panel.

Evidently, the different input energy values greatly affected the endurance of the battery. In Table 31, we show all the calculated and actual test results obtained from testing of the load that represented the Raven with and without the solar panel. Here again, we noted that our computations came very close to the real values obtained from the experiment.

Table 31. Calculated vs. Actual Time.

	Energy IN from SP	Calculated Time	Calculated Improvement
Load w/o SP	0Wh	1h 26min	0%
Raven w/ SP	14.55Wh	2h 13min	54%
Raven w/ SP	16.85Wh	2h 25min	69%
	Energy IN from SP	Actual Time	Actual Im-provement
Load w/o SP	0Wh	1h 29min	0%
Raven w/ SP	14.55Wh	2h 10min	46%
Raven w/ SP	16.85Wh	2h 24min	62%

2. Raven with Solar Panel (100%-55%)

We conducted two tests with the Raven and with solar panel at 100% and 55% throttle. In our first test, we had an average energy input of 13.55Wh. The test was started at around 3:00pm. Unfortunately, 2 hours later the sunny conditions began to deteriorate due to the presence of heavy clouds; hence, we observed a big drop at the end of the test. During our second test, we noticed an average energy input of 12.7Wh. These two energy input values stayed between our calculated range, as previously shown in Tables 20 and 21. The input energy of both test days is shown in Figure 52.

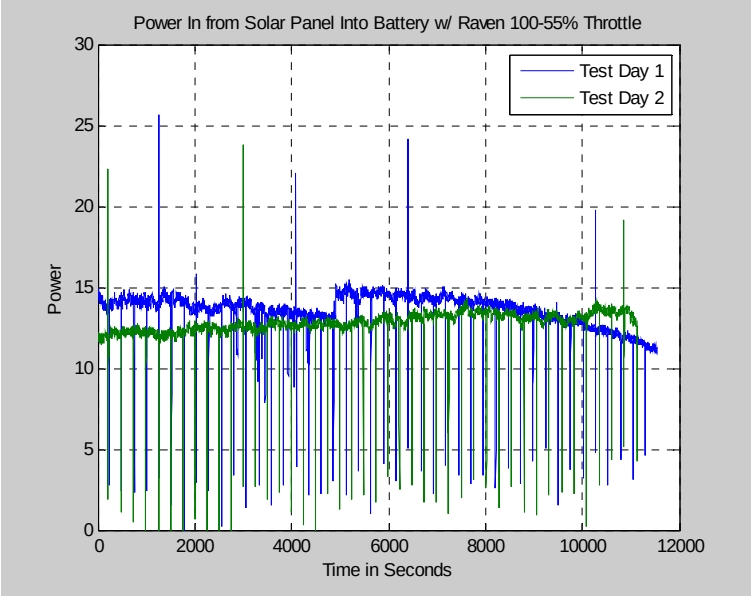

Figure 52. Power Input to Raven w/SP 100%-55% Throttle Test.

In Figure 53, we show the results for the two tests with solar panel and compare them with the original power consumption test performed without the solar panel at 100% to 55% throttle. During the first day, the test lasted 11,540-seconds which corresponded to 3 hours and 12 minutes. During the second day, the test lasted 3 hours and 5 minutes. The difference in time was due to the difference in input energy received from the solar panel on both days, as seen previously in Figure 52.

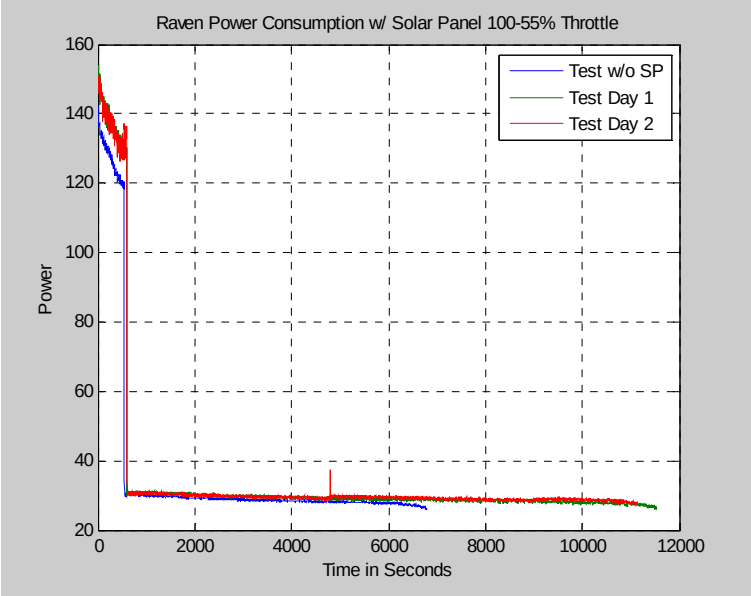

Figure 53. Power Consumption Raven w/SP 100%-55% Throttle.

As in the previous section, we wanted to show the calculated and actual time results at the average energy input levels obtained the day of the tests. These results are shown in Table 32.

Table 32. Actual Time and Improvement.

	Energy IN from SP	Actual Time	Improvement
Load w/o SP	0Wh	1h 53min	0%
Raven w/SP Test 1	13.55Wh	3h 12min	70%
Raven w/SP Test 2	12.70Wh	3h 5min	64%

3. Raven with Solar Panel (100%-65%)

This was the last test to be conducted and by this time, we only had one battery left for the test. The other batteries were accidentally over-discharged and were no longer usable. Moreover, the battery that we used for this test was not holding up the energy. Needleless to say, we carried on with the test to see if even under these condi-

tions, the battery could still last a little longer. We conducted two tests at 100%-65% throttle to see if the endurance time of the battery would fall between the calculated values obtained in Tables 22 and 23. In Figure 54, we noticed that the input energy obtained during the first day of the test averaged 11.94Wh. The average energy input during the second test was 10.62Wh.

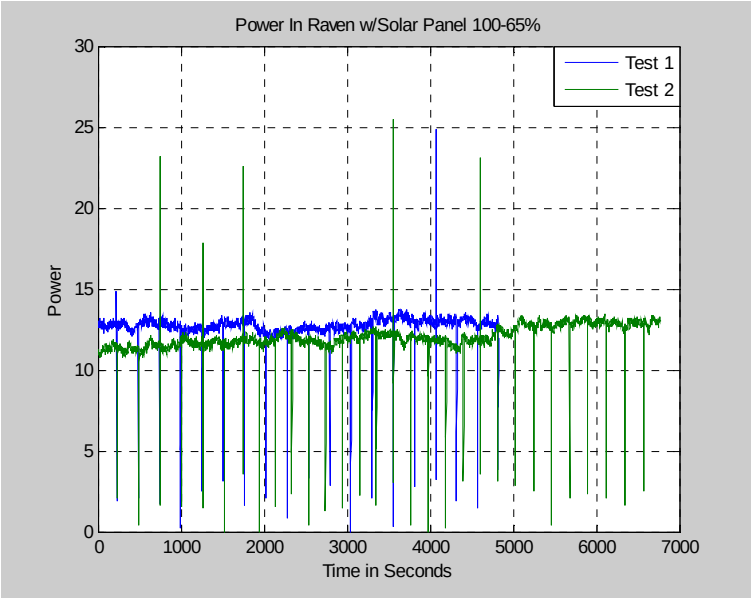

Figure 54. Power Input to Raven w/SP 100%-65% Throttle Test.

In Figure 55, we noticed that the first test with the battery lasted 1 hour and 53 minutes i.e., 19 minutes shorter compared to the projected time of 2 hours and 12 minutes. During the second test, the battery lasted 7,606-seconds which represented 2 hours and 6 minutes, exactly 1-minute longer than expected. However, we also noticed that the power consumption during the initial 10 minutes at 100% was not the same compared to all the other plots. Additionally, we observed a square type signal output that reflected the consumption of the battery. As mentioned be-

fore, we believed that by this time our batteries were reaching their end of their life cycles and we could not continue performing more tests due to the lack of more spare batteries. Although our experiment values did not match our calculated ones, we still observed a small improvement. Nevertheless, we think that more tests need to be done at this throttle setting to demonstrate that our calculation method is accurate.

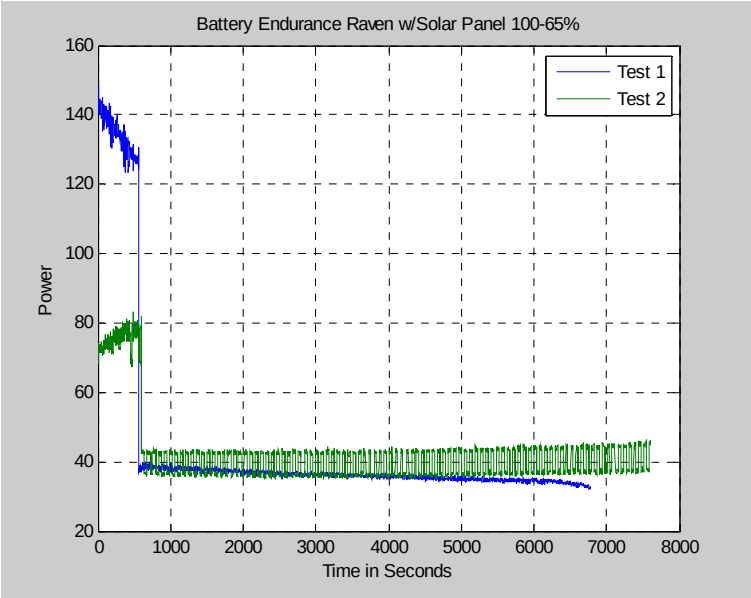

Figure 55. Power Consumption to Raven w/SP 100%-65% Throttle.

The actual time results and improvement observed during the test conducted on the Raven with solar panel at 100% and 65% throttle settings are shown in Table 33.

Table 33. Actual Time Results and Improvement.

	Energy IN from SP	Actual Time	Improvement
Raven w/o SP	0Wh	1h 34min	0%
Raven w/SP Test 1	11.94Wh	1h 53min	20%
Raven w/SP Test 2	10.62	2h 06min	34%

4. Raven with Solar Panel (100%-70%)

When conducting the test at 100% and 70% throttle, we observed an average energy input of approximately 12.5Wh, as seen in Figure 56. .

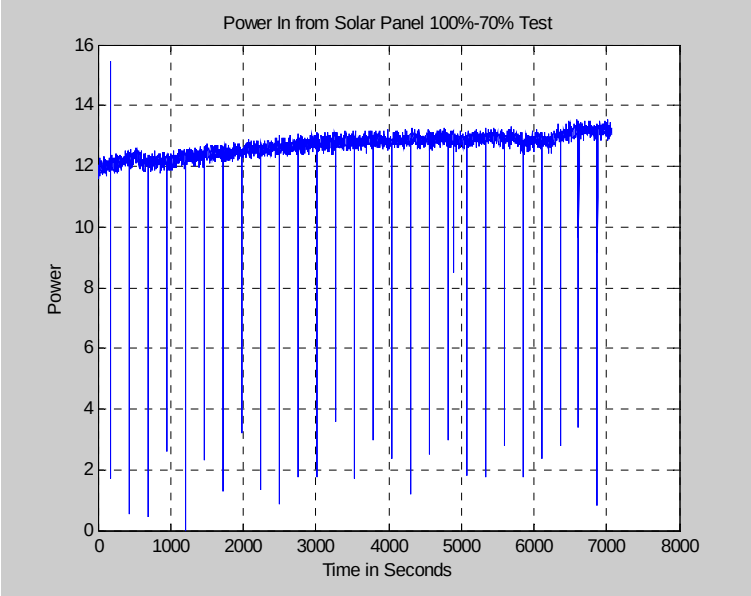

Figure 56. Power Input Raven w/SP 100-70% Throttle Test.

Nevertheless, the duration the test lasted 1 hour 58 minutes, 2 minutes shorter than what we calculated. The overall time that it took for the battery to discharge down to 21.2V is seen in Figure 57.

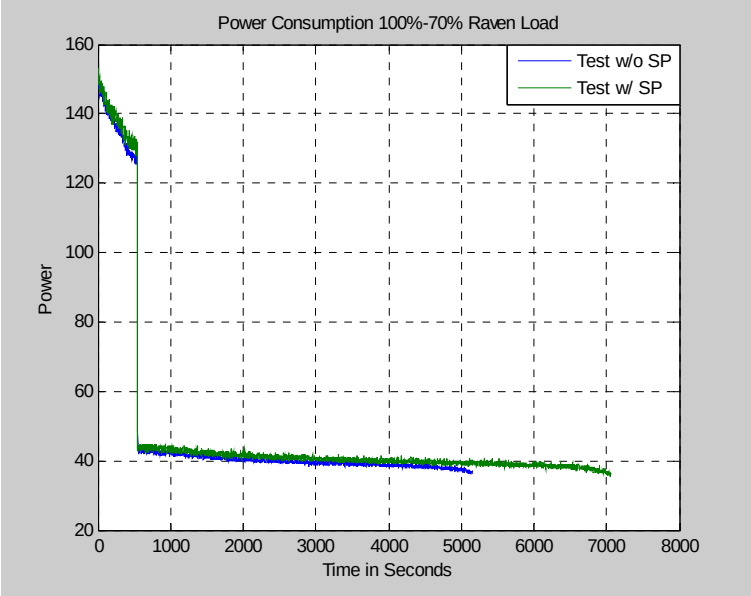

Figure 57. Power Consumption Raven w/SP 100%-70% Throttle.

Again in Table 34, we showed the actual time obtained for the test conducted with the Raven and solar panel at 100% and 70% throttle settings. In this case, we still noticed an improvement of 37%.

Table 34. Actual Time and Improvement.

	Energy IN from SP	Actual Time	Improvement
Raven w/o SP	0Wh	1h 26min	0%
Raven w/SP Test 1	12.55	1h 58min	37%

H. OBSERVATIONS

1. Modified Wing

As mentioned earlier, the tests conducted in this research were based on the inputs provided by the operator of the Raven RQ-11B UAV. It is important to keep in mind that, according to the operator, the Raven UAV requires no

power to descend and that its elongated wing provides more lift; thus, we can expect the endurance of the Raven to be longer.

The modified wing, without solar cells, was tested on 10 May 2010, during a flight demonstration at the Concept-Based Experimentation (CBE) conference at Camp Roberts, California. The flight test lasted an additional time of 34 minutes. Hence, according to the sponsors of the project, the elongated wing improved the flight time by 37% [45]. This means that the improvement in battery endurance could be actually higher than calculated, when the Raven flies with the solar panel and the modified wing.

2. Current Test

After determining the power consumption and the endurance of the battery at 55%, 65%, and 70% throttle settings with the solar panel, we were curious to find out what would be the throttle level in which the solar panel could provide enough energy to run the motor without relying on battery power.

To do this, we connected a third multi-meter between the positive terminal of the battery and the point where the MPPT and the load were connected, as seen in Figure 58.

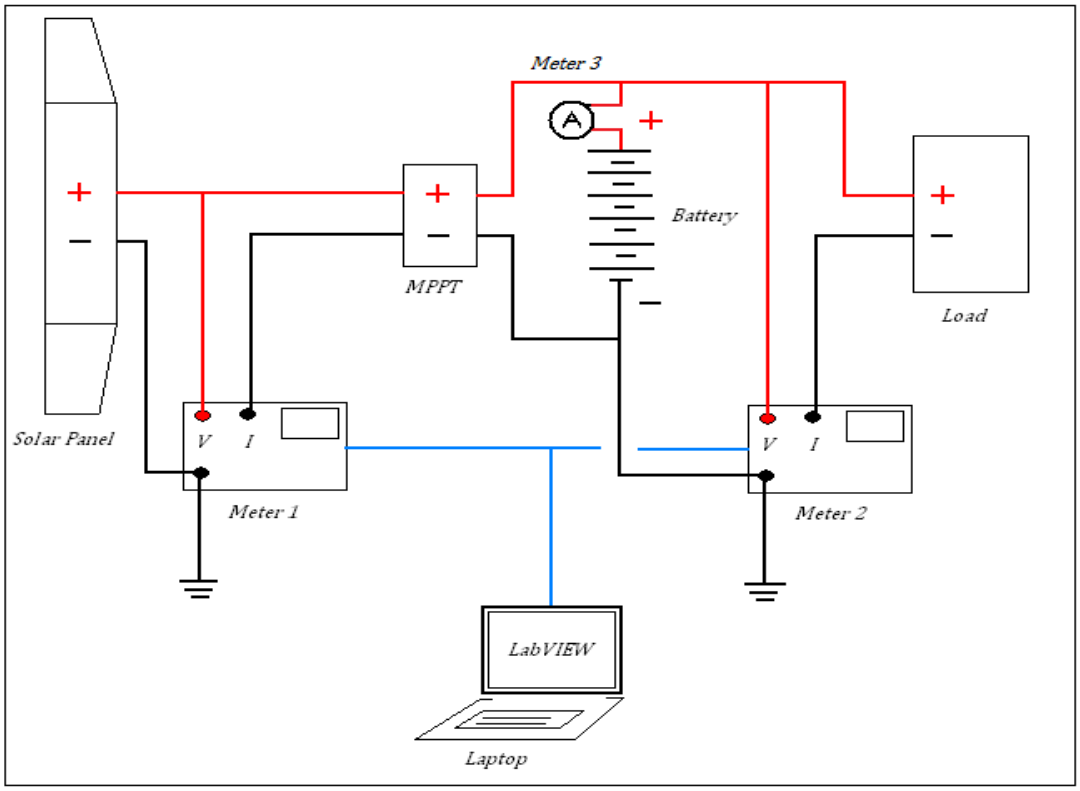

Figure 58. Current Test Connection.

We noted that at 40% throttle the current going into the battery and the current going out from the battery was the same. We also noticed that at 15% throttle the solar panel was actually driving the motor of the UAV and charging the battery.

3. Daily Energy Variations

Unfortunately, these improvements greatly depend on the amount solar energy the wing could absorb during a single mission. The tests conducted in the Monterey area were difficult to do because of the constant presence of clouds in the area. On the other hand, the tests conducted in Carmel Valley, California were more consistent. Therefore, we anticipated that testing the solar panel in areas where

there is a higher index of irradiance, such as the deserts of Africa or Arizona; the improvement could be much higher.

4. Temperature

Another factor that limited our ability to obtain a longer endurance was temperature. Studies have determined that a solar cell loses approximately 2mV for every degree Celsius above room temperature [46]. To prove this fact, we first measure the temperature and the voltage of a single cell under sunlight, while the entire panel was being cooled down by a fan. Using an IR thermometer and a multimeter, we obtained 35-degree Celsius and 23.7V. Then, we placed the solar panel on the floor and block any wind currents to prevent any cooling of the cell. Using the same measurement devices, we obtained 66-degrees Celsius and 21.6V from the same solar cell. It is worth mentioning that the voltage measured was open circuit voltage. Overall, we observed a difference of 29-degrees Celsius and 2.1V between both tests. Using the fact stated in [46] and knowing that we had close to a 30-degree Celsius increase in temperature and 40 cells on the panel, we expected to have a voltage drop of 2.4V. Thus, we confirmed that temperature drastically affected our input power coming from the solar panel by approximately 10%. Luckily, we are confident that temperature would not play a big roll while the solar panel is mounted on the Raven RQ-11B and flying, since it would have sufficient wind to keep the solar cells cool and because temperature decreases as the Raven reaches altitudes above 2,000ft.

5. MPPT Fluctuations

Throughout all of our tests, we observed a constant dip in our input power, as it was seen in Figures 50, 52, 54, and 56. This phenomenon took place every 300-second and became one more factor that lessened the input power provided by the solar panel. On 2 September 2010, we asked the technicians of GENASUN about our constant resetting of the MPPT Boost Charge Controller to find out if it was due to a defective component. They replied saying that the appearance of those dips in the input power is the result of the internal operation of the MPPT. They added that the MPPT Boost charge controller periodically auto-zeroes the current measurement to ensure proper operation at maximum power, but it happens in fractions of a second that has no major impact on the average current of the solar panel. Hence, the device was operating normally [47].

6. Weight

In order to do any modification on the Raven UAV, the Aircraft Controlling Custodian Type Commander (ACC/TYCOM) needs to authorize it, provided that the alteration would not affect the structure and would not impact drastically the weight and balance of the aircraft. For this part of the research, a total of weight of 560gr was authorized to incorporate solar cells onto the Raven UAV [48]. This weight included the modified wing. We weighed the original and the modified wings without solar cells to see the difference between them. The original wing weighed 10.4-Oz (295gr) and the modified wing weighed 18.6-Oz (527gr), i.e., 8.2-Oz (232gr) heavier than the original.

The weight for the solar portion of the project, which includes the solar cell, MPPT, and balancer charger was only 221gr. The overall weight was below the authorized maximum given by the ACC/TYCOM. The breakdown of weights by item is described in Table 35. Therefore, our project complied with the modification request.

Table 35. Final Added Weight.

	Weight (Oz)	Weight (gr)
Solar cells	3.7	105
MPPT	3.6	102
Balancer Charger	0.5	14
Modified Wing	8.2	232
Total	16.0	453

7. Charging Other Batteries

Another part of this research consisted on recharging other batteries using the solar panel as our source of energy. For this portion of the research, we decided to use three Lithium Polymer (Li-po) batteries of 11.1V. Their capacity was 1200mA, 1300mA, and 1350mA. Our solar panel, as described throughout this chapter, gave us an average energy input between 12Wh and 17Wh. During our tests the average input voltage oscillated between 11V and 13V enough voltage to charge 11.1V Li-po batteries. However, since the voltage from the solar panel was higher than the voltage of the batteries, it was necessary to use a MPPT/buck converter that would keep the voltage from overcharging the batteries. The MPPT used for this test was the GV-4 Low Power Charge Controller from GENASUN used in previous thesis work [5]. This MPPT was programmed to charge up to 12.5V. Additionally, we used a balancer charger to ensure that every cell in the battery would charge equally.

First, we discharged each battery using three 10-Ohms resistors connected in parallel. Each battery was discharged to 9.7V. We did not want to go below the minimum battery voltage of 9.6V. Then, we disconnected the load from the battery and connected the solar panel.

The recommended charging rate is C/3, which represents 1/3 of the capacity of the battery. This means that if the capacity was 1200mAh, then charging current rate has to be 400mAh, and it should last 3 hours approximately to fully charge the battery. Nevertheless, our solar panel and MPPT were providing around 1A of charging current, which meant that our charging rate was about 1C.

In all three tests, it took about 1 hour and 20 minutes for the batteries to reach peak voltage of 12.47V, 12.44V, and 12.45V. We used the LED indicators on the balancer charger to determine whether the battery was fully charged or not. This occurred when the charging current reached 9% of the rated current of each battery. We also took voltage readings at the end of the test to verify that the battery reached full charge status. The MPPT also indicated when the battery reached full charge status when the green LED status indicator stopped flashing. In Table 36 we can see the time it took to recharge each battery.

Table 36. Li-po Battery Recharge Time.

Battery	Initial Voltage	Final Voltage	Time
Battery #1	9.7V	12.47V	84-min
Battery #2	9.7V	12.44V	80-min
Battery #3	9.7V	12.45V	88-min

Since our charging rate current was higher than recommended, it shortened the charging time compared to other

tests conducted in similar research [5]. In the end, the solar panel successfully charged the two Li-po batteries.

8. Specific Energy Calculation

Our intent was to leave the reader of this thesis research with the idea of how much of a specific energy per weight ratio should be needed to achieve longer flight time.

First, we considered the energy consumed by the Raven with its original payload. Since, the weight of the Raven was 4.2-lbs (1.9Kg) and the energy used in 1 hour and 50 minutes at 100% and 55% throttle configuration was 72.08Wh, we obtained a ratio of 0.038, as seen in equation 6.6.

$$E_{nergy\ per}W_{eight} = \frac{E_{used}}{W_{eight}} = \frac{72.08Wh}{1902.6g} = 0.038 \qquad (5.10)$$

Second, we then considered the same energy consumed by the Raven with the original payload, but we included the modification in support structure, i.e., the modified wing. In this case, since the flight time was 2 hours and 4 minutes, the energy consumed was actually lower (69.28Wh). Moreover, the weight of the modified wing was also heavier by 232g. As a result, the specific energy per weight ratio turned out to be 0.032, as seen in equation 6.7.

$$E_{nergy\ per}W_{eight} = \frac{E_{used}}{W_{eight}} = \frac{69.28Wh}{2134.6g} = 0.032 \qquad (5.11)$$

Finally, we obtained a third specific energy per weight ratio that included the energy consumed by the Raven with the payload, modified wing, and the solar modification circuit. However, in equation 6.8, we noticed that the energy used by the Raven was zero because it flew 3 hours,

i.e., 1 hour and 10 minutes longer without using a single Watt hour of energy from the battery.

$$E_{nergy\ per}W_{eight} = \frac{E_{used}}{W_{eight}} = \frac{0Wh}{2355.6g} = 0.0 \qquad (5.12)$$

With this calculation, we could say that the lower the specific energy per weight ratio is, the more flight time improvement we can get. Nevertheless, this is true only if the added weight includes support structure that could improve the lift and/or solar modification that could reduced the amount of energy used from the battery.

I. FLIGHT TEST RESULTS

Unfortunately, we were not able to test our design during flight due to a lack of Raven assets authorized to fly with the solar wing. However, the next opportunity to proof-our concept flight would be in November 2010 at Camp Roberts, during the next CBE Conference.

J. COST ESTIMATE

The amount of money spent on solar cells and other components necessary to conduct this research was only a small fraction of the tag price for a single Raven UAV, which is about $35,000.00. A breakdown of the money spent on this project is described in Table 37.

Table 37. Solar Modification Cost.

	Minimum Purchase Order			Expenditure per Unit	
Item Description	Unit of Issue	Qty	Price	Qty Used	Cost
CIGS Solar Cells (19 cells per string)	String	50	$5,000.00	1	$100.00
Boost MPPT Charge Controller	EA	1	$255.00	1	$255.00
Balancer Charger	EA	1	$29.95	1	$29.95
Carpet Protection Film	Roll	1	$45.99	1	$45.99
Connector	EA	1	$1.99	1	$1.99
Wiring	Spool	1	$6.00	1	$6.00
Copper Conductor Tape	Roll	1	$25.86	1	$25.86
Miscellaneous					$50.00
				Subtotal	$514.79
Labor and Assembly					$500.00
				Total	$1,014.79

Global Solar Energy Inc., the manufacturer of CIGS TFPV cells, could not sell individual strings. Therefore, we were required to purchase a minimum order of 50 strings. Nonetheless, we calculated that the entire solar modification to the Raven RQ-11B could cost around $1,000.00. This represented only 3% of the cost of a single Raven asset, which made this research cost effective.

In this estimate, we did not include the cost for the modification of the wing, since it was modified by the mechanical engineers of the Naval Weapons Center in China Lake, California.

THIS PAGE INTENTIONALLY LEFT BLANK

VII. CONCLUSIONS

In this thesis research, we looked at the entire Raven RQ-11B UAV Program and examined the benefits as well as the limitations provided to ground forces fighting in urban terrain. Throughout this research we examined the beginnings of the Raven UAV, different prototypes built, system configuration and capabilities, cost per unit, training, etc. We intended to give the reader a good appreciation of the potential and incredible advantages that this particular unmanned aerial vehicle gives to the military.

Next, we briefly submerged ourselves into the intricate world of solar cells; specifically, CIGS solar cells. We wanted to get a better understanding of their operation, structure, factors that affect their performance, and the advantages of using thin film photovoltaic cells. We demonstrated that in order to achieve the highest improvement in battery endurance, we ought to seek the highest efficiency CIGS TFPV cells available in today's market. We were fortunate to find 13% efficient CIGS cells.

Additionally, we spent some time looking into other power electronic devices that required to be integrated into our research. We examined their operation, functionality, characteristics, but for the most part, we focused on how they contributed to give us the maximum output power from our solar panel.

The design and assembly of our solar wing panel was, perhaps, the pinnacle of this research. It was essential to come up with the most efficient solar cell arrangement to cover every single area available on the wing. Such ar-

rangement entailed minimizing labor by reducing the number of cuts and connections, and maximizing the output power. Here, we also explained the challenges encountered when working and handling uncovered CIGS TFPV cells. Although it was a tedious and time consuming process, it was a necessary step to avoid damaging the cells and adding more weight to the aircraft. Furthermore, we discussed the incorporation of additional power electronic devices necessary to obtain the power required to charge the battery while on flight.

To proof our concept, we conducted tests at different throttle configurations to match the normal operation of the Raven UAV during regular missions. Our tests were conducted inside our laboratory, initially, and then outdoors to measure the improvements obtained from the solar panel. We made an effort to take readings at different locations where the average energy input was higher.

In this thesis, we also performed a cost benefit analysis to determine how costly it could be to make this solar modification. We determined that the entire modification would cost $1,000.00, which represented only 3% of the cost for a single asset.

In the end, although the weather conditions where our tests were conducted were not favorable for this type of research, we observed a considerable endurance improvement by using solar cells on the wing of the Raven UAV, which validated our thesis. A summary of the results obtained is shown in Table 38.

Table 38. Summary of Testing Results.

100% - 55% Throttle Test			
	Energy IN from SP	Actual Time	Improvement
Raven w/o SP	0Wh	1h 53min	0%
Raven w/SP Test 1	13.55Wh	3h 12min	70%
Raven w/SP Test 2	12.70Wh	3h 5min	64%
100%-65% Throttle Test			
Raven w/o SP	0Wh	1h 34min	0%
Raven w/SP Test 1	11.94Wh	1h 53min	20%
Raven w/SP Test 2	10.62	2h 06min	34%
100% - 70% Throttle Test			
Raven w/o SP	0Wh	1h 26min	0%
Raven w/SP Test 1	12.55	1h 58min	37%

In Table 38, we compared the different tests performed with the solar panel to the tests conducted without the solar modification at those specific throttle configurations. We noticed that under low average energy input conditions we obtained somewhere around 70% improvement when operating between 100% and 55% throttle, and around 40% when operating at the other throttle configurations. We truly believed that more tests are needed at higher average energy input levels to observe improvements equal or greater than 100% at any throttle setting.

A. RECOMMENDATIONS

Although this thesis has proven that the application of CIGS TFPV improves the flight endurance of the Raven UAV, there is more that could be done to optimize our findings.

1. Eliminate Boost Converter

Since the voltage provided by the solar panel was lower than the voltage of the battery, it was imperative to find a DC-DC converter that would step up the voltage from the solar panel to 25.2V to charge the battery. To our benefit, the MPPT that we chose came with a boost converter built-in on the same circuit. The efficiency of this device, according to the manufacturer [41], was 96% to 98%; hence, it loses between 4% to 2% while stepping up the voltage. Adding more cells to the solar panel would increase the voltage to a point where no power converter would be required, and thus, improving the efficiency of the MPPT.

To do this, the area of the solar cells would need to be shorter. However, making the area of the solar cells shorter also implies that the output current would be reduced. Moreover, it becomes more challenging since there are not that many center conductors available on top of the solar cell that could be used to connect them with one another. Therefore, the cell would have to be cut around the center conductors to ensure that each cell would have a place to connect to another cell. Unfortunately, many solar cells would be sacrificed to make others work, resulting in wasteful use of solar cells and added cost to the modification. Without a doubt, it is a difficult task, but it is also one that could bring positive results.

2. Solar Design for Original Wing

The advantage of having a modified wing is that it provides more room to place more solar cells. However, there is also a big disadvantage that most battalion commanders in the battlefield are not willing to take. Un-

less, mechanical engineers find a way to make the modified wing a man-portable item, it would not be accepted by operational units in the field. Thus, there still a need to apply this concept on the original size wing, which has a smaller area. Once again, for this case the area of the solar cells would also need to be shorter to increase the voltage of the solar panel. In addition it would be necessary to make each detachable piece of the center wing and the horizontal stabilizer a separate solar panel with the same number of solar cells connected in series, and the panels connected in parallel. This would give the same output voltage, but it would also increase the amount of current.

3. New Technology CIGS and Power Electronics

Technology is constantly moving at a fast rate. In the area of CIGS TFPV cells, huge improvements in efficiency are being observed every day. As explained in Chapter III, up to 20.1% efficient CIGS cells have been attained [19]. This is an indication that in the near future the manufacturing industry would be able to produce higher efficient cells that would allow us to obtain better results on applications similar to the one conducted on this thesis. Similarly, power electronic devices, such as the ones used in this thesis research, would be available in smaller dimensions and perhaps with higher efficiency. This is the case of the SPV1020 boost converter from STMicroelectronics, which is a single chip that uses a combination of a DC-DC converter with a digital logic circuit to perform as an MPPT. This device is designed to increase the efficiency of solar panels [49].

THIS PAGE INTENTIONALLY LEFT BLANK

LIST OF REFERENCES

[1] R. J. Boucher, "History of solar flight," presented at *AIAA/SAE/ASME 20th Joint Propulsion Conference*, Cincinnati, OH, 1984.

[2] Joseph, Flatley, “Zephyr solar UAV sets yet another flight record: 7 days and counting!” *Engadget.* Jul. 2010. [Online]. Available: http://www.engadget.com/2010/07/17/zephyr-solar-uav-sets-yet-another-flight-record-7-days-and-coun/. [Accessed Jul. 31, 2010].

[3] Global Security, “High altitude airship (HAA),” *Global Security.* May 2008. [Online]. Available: http://www.globalsecurity.org/intell/systems/haa.htm. [Accessed 4 June 2010].

[4] Martha Falconi, “Solar plane passes big test, flies 24 hours straight.” *AOL News.* Jul. 2010. [Online]. Available: http://www.aolnews.com/tech/article/solar-impulse-plane-powered-by-the-sun-lands-safely-after-24 hour-test-flight/19546048. [Accessed 11 July 2010].

[5] William Hurd, “Application of cupper indium gallium diselenide photovoltaic cells to extend the endurance and capabilities of unmanned aerial vehicles,” M.S. thesis, Naval Postgraduate School, Monterey, CA, 2009.

[6] Global Security, “RQ-11 raven,” Apr. 2005. [Online]. Available: http://www.globalsecurity.org/intell/systems/raven.htm. [Accessed 17 July 2010].

[7] Directory of U.S. Military Rockets and Missiles, “AeroVironment FQM-151 pointer,” *Designation-Systems.* Jan. 2006. [Online]. Available: http://www.designation-systems.net/dusrm/index.html. [Accessed 24 July 2010].

[8] A. Mawn and P. Tokamaru, “The pathfinder raven small unmanned aerial vehicle,” in *Proc. Of 24th Army Science Conf. 2004.* [Online]. Available: http://handle.dtic.mil/100.2/ADA432526. [Accessed 1 August 2010].

[9] Directory of U.S. Military Rockets and Missiles, “AeroVironment RQ-11,” *Designation-Systems.* Sep. 2006. [Online]. Available: http://www.designation-systems.net/dusrm/app2/q-11.html. [Accessed 24 July 2010].

[10] United States Army. “RQ-11B raven small unmanned aircraft system (SUAS).” Mar. 2010. [Online]. Available: http://www.rucker.army.mil/docs/usaace_info/USAACE%20Info%20Paper%20TCM-UAS%20RQ-11B%20Raven%20UAS%2022%20Mar%2010.pdf. [Accessed 25 July 2010].

[11] Army Technology, “RQ-11 raven unmanned aircraft system, USA.” *Army-Technology*. 2010. [Online]. Available: http://www.army-technology.com/projects/rq11-raven. [Accessed 17 July 2010].

[12] Unmanned Aerial System, “Raven RQ-11B,” *Unmanned Aerial System.* 2009. [Online]. Available: http://www.af.mil/shared/media/photodb/photos/070706-f-6751b-204.jpg. [Accessed 24 July 2010].

[13] John Keller, "Unmanned vehicle spending in the 2010 dod budget to reach $5.4 billion." *Military and Aerospace Electronics.* Dec. 2009. [Online]. Available: http://www.militaryaerospace.com/index/display/article-display/363553/articles/military-aerospace-electronics/executive-watch/unmanned-vehicle-spending-in-the-2010-dod-budget-to-reach-54-billion.html.[Accessed 10 July 2010].

[14] U.S.Army, “U.S. army roadmap for UAS 2010-2035.” *Stand-To.Army*. Apr. 2010. [Online]. Available: http://www.rucker.army.mil/usaace/uas/U.S.%20Army%20UAS%20RoadMap%202010%202035.pdf. [Accessed 17 July 2010].

[15] B. Cossel, “Raven pre-flight checks,” *Defend America.* Oct. 2004. [Online]. Available: http://www.defendamerica.mil/photoessays/oct2004/p101904b1.html. [Accessed 1 August 2010].

[16] J. Glenn and W. Snodgrass, ”The Raven small unmanned aerial vehicle (SUAV), investigating potential dichotomies between doctrine and practice.” M.S. Thesis, Naval Postgraduate School, Monterey, CA, 2005.

[17] Operator and Field Maintenance Manual, *“Small unmanned aircraft system (SUAS) RQ-11B NSN 1550-01-538-99256.”* Department of the Army. 2008.

[18] K. Ramanathan, J. Keane, and R. Noufi, “Properties of high-efficiency cigs thin-film solar cells.” *National Renewable Energy Laboratory*. Feb. 2005. [Online]. Available:http://www.nrel.gov/docs/fy05osti/37404.pdf. [Accessed 24 July 2010].

[19] M. Osborne. “CIGS record of 21% efficiency reported by researchers at ZSW,” PV-Tech. Apr. 2010. [Online]. Available: http://www.pv-tech.org/news/_a/cigs_record_of_20.1_efficiency_reported_by_researchers_at_zsw/. [Accessed 24 June 2010].

[20] Global Solar Energy, “G2 thin film string data sheet,” *Global Solar.* Jul. 2010. [Online]. Available: http://www.globalsolar.com/en/products/cigs-thin-film-material.html. [Accessed 30 August 2010].

[21] Christiana Honsberg and Stuart Bowden, *PVCDROM.* Aug. 2010. [Online]. Available: http://www.pveducation.org/pvcdrom. [Accessed 29 August 2010].

[22] Eppley Laboratory, “What is solar radiation?” *Discover Solar Energy.* Jul. 2008. [Online]. Available: http://www.discoversolarenergy.com/solar/radiation.htm. [Accessed 29 August 2010].

[23] Newport, “Air mass conditions,” *Opto IQ.* May. 2009. [Online]. Available: http://www.optoiq.com/index/photonics-technologies-applications/lfw-display/lfw-article-display/361941/articles/laser-focus-world/features/photovoltaics-measuring-the-sun.html. [Accessed 29 August 2009].

[24] Renewable Energy, “Band gap diagram with photovoltaic effect,” *Durham University*. Aug. 2010. [Online]. Available: http://www.dur.ac.uk/images/renewable.energy/pvfig3.gif. [Accessed 29 August 2010].

[25] “Solar cell: structure,” *Encyclopedia Britannica.* 2005. [Online]. Available: http://www.britannica.com/EBchecked/topic-art/552875/1406/A-commonly-used-solar-cell-structure. [Accessed 29 August 2010].

[26] “Cooper indium gallium selenide,” *Wikipedia*. Aug. 2010. [Online]. Available: http://en.wikipedia.org/wiki/Copper_indium_gallium_selenide. [Accessed 17 July 2010].

[27] I. Repins, M. Contreras, B. Egaas, C. Dehart, J. Scharf, C. Perkins, B. To, R. Noufi, "19.9%-efficient ZnO/CdS/CuInGaSe2 solar cell with 81.2% fill factor". *Progress in Photovoltaics: Research and applications.* 2008. [Online]. Available: doi:10.1002/pip.822. [Accessed 29 August 2010].

[28] U. Malm,”Modelling and degradation characteristics of thin-film CIGS solar cells,” Ph.D. dissertation, Uppsala Universitet, Uppsala, Sweden, 2008.

[29] Y. Yan, D. Albin, and M. Al-Jassim,“The effects of oxygen on junction properties in CdS/CdTe solar cells,” *National Renewable Energy Laboratory*. Presented at NCPV Program Review Meeting, Colorado, October 2001. [Online]. Available: http://www.nrel.gov/docs/fy02osti/31036.pdf. [Accessed 22 July 2010].

[30] R. Noufi and K. Zweibel, “High-efficiency CdTe and CIGS thin-film solar cells: highlights and challenges,” in *4th World IEEE Conference On Photovoltaic Energy,* 2007.

[31] Wikipedia,“Boost converter,” *Wikipedia*. Aug. 2010. [Online]. Available: http://en.wikipedia.org/wiki/Boostconverter. [Accessed 8 August 2010].

[32] Dorf, Richard, “The engineering handbook.” 2nd Ed. Boca Raton: CRC Press, 2004, pp.175.

[33] Richard A. Cullen, “Frequently asked questions& technical tips.” *Blue Sky Energy Inc*. Apr. 2004.[Online]. Available: http://www.blueskyenergyinc.com/uploads/pdf/BSE_What_is_MPPT.pdf. [Accessed Aug. 9, 2010].

[34] M.J. Isaacson, R.P. Hollandsworth, P.J. Giampaoli, F.A.Linkowsky, A. Salim, and V.L. Teofilo, “Advanced lithium ion battery charger.” *IEEE Explore.* Aug. 2002. [Online]. Available: http://ieeexplore.ieee.org/stamp/stamp.jsp?tp=&arnumber=574108. [Accessed 9 August 2010].

[35] Cadex Electronics, “Is lithium-ion the ideal battery?” *Cadex Electronix Inc.* 2005. [Online].Available: http://www.batteryuniversity.com/partone-5.htm. [Accessed 29 August 2010].

[36] A. Moore, “Lithium polymer (lipo) battery guide,” *Prototalk.* Nov. 2008. [Online]. Available: http://prototalk.net/forums/showthread.php?t=22. [Accessed Aug. 29, 2010].

[37] Gilbert Magana (gilberto.magana@navy.mil), “Re: Composite wing,” July 27,2010.

[38] Global Solar Energy,“G2 thin film string datasheet,” Global Solar. July 2008.

[39] Plasticover, “Carpet protection film,” *Plasticover*. 2010. [Online]. Available: http://www.plasticover.com/protector/carpet-protector.html. [Accessed 6 August 2010].

[40] Wire Glue, “Wire glue,” *Wire Glue*. 2010. [Online]. Available: http://www.wireglue.us. [Accessed 8 August 2010].

[41] GenaSun, “GV-boost specifications,” *GenaSun.* 2010. [Online]. Available: http://www.genasun.com/gvb.shtml. [Accessed 7 August 2010].

[42] National Instruments, “*Introduction to labview and computer-based measurements hands-on seminar*,” National Instruments; Ed. January 2010.

[43] S. Brown (private communication), 2010.

[44] PowerStream. “How to calculate battery run-time,” *PowerStream*. [Online]. Available: http://www.powerstream.com/battery-capacity-calculations.htm. [Accessed 10 August 2010].

[45] S. Thompson (private communication), 2010.

[46] Sherif Michael, “EC2320 space power and radiation effects solar basics,” 2009. [Class Notes – Unpublished].

[47] A. Hayman (Hayman@genasun.com), “Re: Technical question about GVB26-4,” September 2, 2010.

[48] “Raven/RQ-11B Aircraft Modification Request,” Naval Air Warfare Center Weapons Division, China Lake, California, VX-31-2010-00027, March 2010.

[49] STMicroelectronics. “Interleaved DC-DC boost converter with built-in MPPT algorithm,” *STMicroelectronics.* [Online]. Available: http://www.st.com/stonline/products/literature/ds/17588.pdf. [Accessed 9 September 2010].

INITIAL DISTRIBUTION LIST

1. Defense Technical Information Center
   Ft. Belvoir, Virginia

2. Dudley Knox Library
   Naval Postgraduate School
   Monterey, California

3. Marine Corps Representative
   Naval Postgraduate School
   Monterey, California

4. Director, Training and Education, MCCDC, Code C46
   Quantico, Virginia

5. Director, Marine Corps Research Center, MCCDC, Code C40RC
   Quantico, Virginia

6. Marine Corps Tactical Systems Support Activity (Attn: Operations Officer)
   Camp Pendleton, California

7. Dr. R. Clark Robertson, Chairman
   Department of Electrical and Computer Engineering
   Naval Postgraduate School
   Monterey, California

8. Dr. Sherif Michael
   Department of Electrical and Computer Engineering
   Naval Postgraduate School
   Monterey, California

9. Dr. Todd Weatherford
   Department of Electrical and Computer Engineering
   Naval Postgraduate School
   Monterey, California